Common Cyclicities in Seismicity and Water Level Fluctuations at the Charlevoix Seismic Zone of the St. Lawrence River

by

Georgios Padelis Tsoflias

Thesis submitted to the Faculty of the

Virginia Polytechnic Institute and State University

in partial fulfillment of the requirements for the degree of

Masters of Science

in

Geophysics

APPROVED:

Gilbert A. Bollinger, Chairman

John K. Costain

Edwin S. Robinson

Robert J. Wetmiller

August 7, 1991

Blacksburg, Virginia

Common Cyclicities in Seismicity and Water Level Fluctuations

at the Charlevoix Seismic Zone of the St. Lawrence River

by

Georgios Padelis Tsoflias

G. A. Bollinger, Chairman

Geophysics

(ABSTRACT)

Intraplate seismicity has no widely accepted explanation for its origin. The Hydroseismicity hypothesis, developed by Costain and co-workers, suggests that natural increases in hydraulic head, caused by transient increases in water table elevation, can be transmitted to hypocentral depths (10-25 km) in a fractured, prestressed, near-failure crust, and along with long term hydrolitic weakening of rocks, contribute to the triggering of earthquakes. In this study, the temporal characteristics of seismicity and water level fluctuations at the Charlevoix seismic zone on the Saint Lawrence river are investigated to provide a test of the Hydroseismicity hypothesis.

To characterize the temporal release of seismic energy, two measures of seismic activity are considered for the available 200 year record of seismicity: the strain factor (magnitude dependent), and the number of events per unit time (magnitude independent). Residual analysis, applied to the strain factor time series, indicates a cyclical variation of the seismicity with long term periods ranging from 65 to 70 years. Fourier spectral analysis, applied on both strain factor and number of events time series, indicates the presence of short term cyclicities of seismic energy release at 13 to 14 year periods, along with longer term cyclicities of approximately 55 to 70 year periods. Fisher's periodogram ordinate test, applied to the spectral analyses results to determine the significance of the largest periodogram ordinate with respect to the average, tested the 13.4 year periodogram ordinate of the number of events time series significant at the 10% level, whereas the 13.4 year periodogram ordinate of the strain factor time series failed to test statistically significant.

Analysis of the residual water level 70 year long time series indicates a cyclical process with quarter cycles of approximately 20 years, suggesting a complete cycle of 70 to possibly 80 years. Fourier spectral analysis of the water level data set indicates cyclicities with periods of 1, 23, 14 and 8 years. The Grenander-Rosenblatt method (Priestley, 1981), applied to the spectral analysis results, tests the statistical significance of the largest periodogram ordinates, and showed the 1, 23, 14 and 8 year periodogram ordinates to be significant at the 1% level.

Cyclicities present in the water level and seismicity time series were investigated for temporal (time lag) relationships using Group Delay analysis, a procedure that tests for time relationships at selected bandwidths. The maximum value of the Group Delay function occurs at the 14 year period with a time lag of +2.3 years, indicating that the water levels lead the seismicity time series. The crustal diffusivity values estimated from the Group Delay analysis of the 14 year center period, range between 0.3 m^2/sec and 2.7 m^2/sec for a depth interval from 7 to 20 km. Direct correlation between depth and crustal diffusivity is not justified with the data at hand; however, the range of estimated diffusivities is within the range of published values of diffusivities for the crust (0.1 to 100 m^2/sec).

This study allows for a possible causal relationship between repetitive mechanical effects of pore pressure transients and seismicity in the Charlevoix seismic zone. The temporal behavior of the physical processes studied is in general agreement with the Hydroseismicity model.

Acknowledgements

I would sincerely like to thank my advisor Dr. Bollinger, for his continuous support and guidance throughout my graduate studies, and for the great opportunity he has given me to be an active member of the Seismological Observatory at Virginia Tech. My educational and professional gains have been tremendous. Special thanks are extended to Dr. Costain, for his continuous discussions on methods and results throughout my thesis research, which, along with his enthusiasm, made this project a really stimulating and worth investigating subject. I am thankful to Dr. Robinson, and Dr. Wetmiller of the Geological Survey of Canada, for their critical reviews of my thesis and for their willingness to participate in the examining committee of my thesis.

I would like to thank Matt Sibol for his assistance with the use of the Seismological Observatory data base and the computer facilities, and Martin Chapman for his helpful suggestions on my research. Furthermore, I would like to thank Dr. Snoke, and Dr. Çoruh my undergraduate advisor, whose classes broadened my geophysical background.

I am grateful to the Water Survey of Canada, and in particular to Mr. P.J. McCurry and Mr. M. Miron, who provided the hydrometric data. I am also grateful to the Geological Survey of Canada, especially to Mr. B. Shannon, who provided the seismicity data. Without their cooperation, this study would have not been possible.

Finally, I would like to thank Miss D. Woodward and Mr. T. Woodfield of SAS Institute Inc., for their helpful suggestions with the SAS system.

Table of Contents

List of Illustrations

List of Tables

Introduction

The origin of intraplate seismicity is not well understood at present. Hydroseismicity is a hypothesis developed by Costain and co-workers (1987a,b, 1988, 1991) that deals with the role of meteoric water in the generation of some intraplate seismicity. The hypothesis suggests that natural increases in hydraulic head, caused by transient increases in water table elevation, can be transmitted to hypocentral depths (10-25 km) in a fractured and suitably prestressed crust, and thereby contribute to the triggering of earthquakes. Although Hydroseismicity is not considered to be the primary driving force in intraplate seismicity, it is believed to play a key role in the triggering mechanism for at least some intraplate earthquakes.

Three essential component elements comprise the Hydroseismicity model: Large groundwater basins with relatively high hydraulic gradients, a rifted upper crust, and a strong in situ-stress field.

Some large ground water basins, that occur in the eastern North America, are spread over large fractured crustal volumes of 100-200 km width by several hundred kilometers length. Vertically, the fractures extend in depth down to the brittle-ductile transition (18 - 25 km). When high average stream gradients are present, they can provide the basin with an efficient, gravity-driven ground water flow. The geometry of the flow-path in such basins is presumed to be similar to the one encountered in any ground water basin (Freeze and Cherry, 1979), except for the scale. As observed by Costain et al. (1987b), such major river basins also host active seismicity in many cases. For example, the Broad, Congaree, Cooper river system occur in the South Carolina-Georgia seismic zone; the James river bisects the central Virginia seismic zone; the New River in Virginia bisects the Giles County seismic zone; the Tennessee river and its tributaries intersect the eastern Tennessee seismic zone; the Mississippi river bisects the New Madrid seismic zone; and the Saint Lawrence river intersects the Charlevoix seismic zone (Figure 1). It should be noted that not all large ground water basins are in seismically active areas, presumably because of the absence of suitable subsurface geologic conditions, i.e. adequate fracture permeability, adequate topographic relief to provide hydraulic gradients, and/or high levels of in-situ stress.

A rifted crust is essential in the model because it provides the fracture permeability required for the ground water flow and pore pressure diffusion paths down to hypocentral depths. There is ample of evidence of such fracture permeability to depths of 15 - 20 km as reviewed by Costain et al. (1987a,b) and Costain and Bollinger (1991). Values of permeability in crystalline rocks range from 10^{-14} to 10^{-9} cm^2 as determined from direct in situ (drill holes $\cong$ 2-3 km) and laboratory experiments. In cases of reservoir induced seismicity, earthquake migration patterns around large reservoirs have indicated crystalline rock permeabilities of 10^{-12} to 10^{-10} cm^2.

A strong in situ stress field is required so that the volume of rock is strained and close to failure. Transient elevations of the water table, due to increased rainfall, results in fluid pressure transients that are diffused downward to hypocentral depths (10-25 km). This mechanical effect along with long term chemical weakening of the rocks due to the continual presence of water, is postulated to trigger the release of preexisting stress.

Extensive research on the interaction of water and seismicity has shown that pore pressure changes, due to reservoir filling or water level changes, in a suitable geologic setting can generate seismicity. Seismicity has been known to be induced by the filling of some reservoirs, for example, at Nurek (U.S.S.R), Oroville (U.S.A), and Aswan (Egypt) (Simpson, 1976; 1987; Simpson and Negmatullaev, 1981). Leblanc and Anglin (1978) reported a case of induced seismicity at the Manic

3 reservoir in Quebec, Canada, some 150 km to the northeast of the Charlevoix seismic zone. After investigations at Monticello Reservoir in South Carolina, Talwani and Acree (1985), suggested that changes in pore pressure diffused to hypocentral depths were the primary causes of observed seismicity. Water injection at wells has also been known to induce seismicity, as exhibited by the disposal well at the Rocky Mountain Arsenal near Denver Colorado (Evans, 1966). The seismicity induced by the filling of reservoirs and the injection of water in wells was of shallow depth and resulted from large pore pressure changes (tens to few hundreds of bars) over short periods of time (months to hours) (Talebi and Cornet, 1987). It is believed that Hydroseismicity shares common elements with the above phenomena. The repetitive small pore pressure changes ($\cong$ 1 bar) over large periods of time (years) can be transmitted to focal depths in fractured crystalline rocks, and, in concert with possible chemical weakening, trigger seismicity.

Three possible Hydroseismicity trigger mechanisms may be considered at present: Transient mechanical effects due to pore pressure transients; Reduction of the shear strength of rocks due to chemical effects; Combination of static stresses and mineral dissolution. Repetitive pore pressure changes can raise the shear stress, and in a near failure environment, cause seismicity. Nava's (1983) study of naturally induced seismicity in the New Madrid seismic zone by the Mississippi river, suggests that small pore pressure changes (fraction of a bar) can trigger seismicity. Furthermore, chemical dissolution resulting in weakening of rocks, over long periods of time, could also contribute to seismicity. The temporal characteristics of the Hydroseismicity process might be determined primarily, but not completely, by the mechanical effects, since the chemical effects are acting continuously on the rocks.

Evidence supporting the Hydroseismicity hypothesis comes from correlations found between variations in Mississippi river stage and seismicity in the New Madrid seismic zone (Nava and Johnston, 1984). Also Costain and Bollinger (1991), found 10-30 year period cyclicities in both the residual streamflow in the James river and the seismicity in the central Virginia seismic zone. In this study, cyclicities in seismicity and water level fluctuations at the Charlevoix seismic zone on the Saint Lawrence river will be investigated to provide another test of the Hydroseismicity hypothesis.

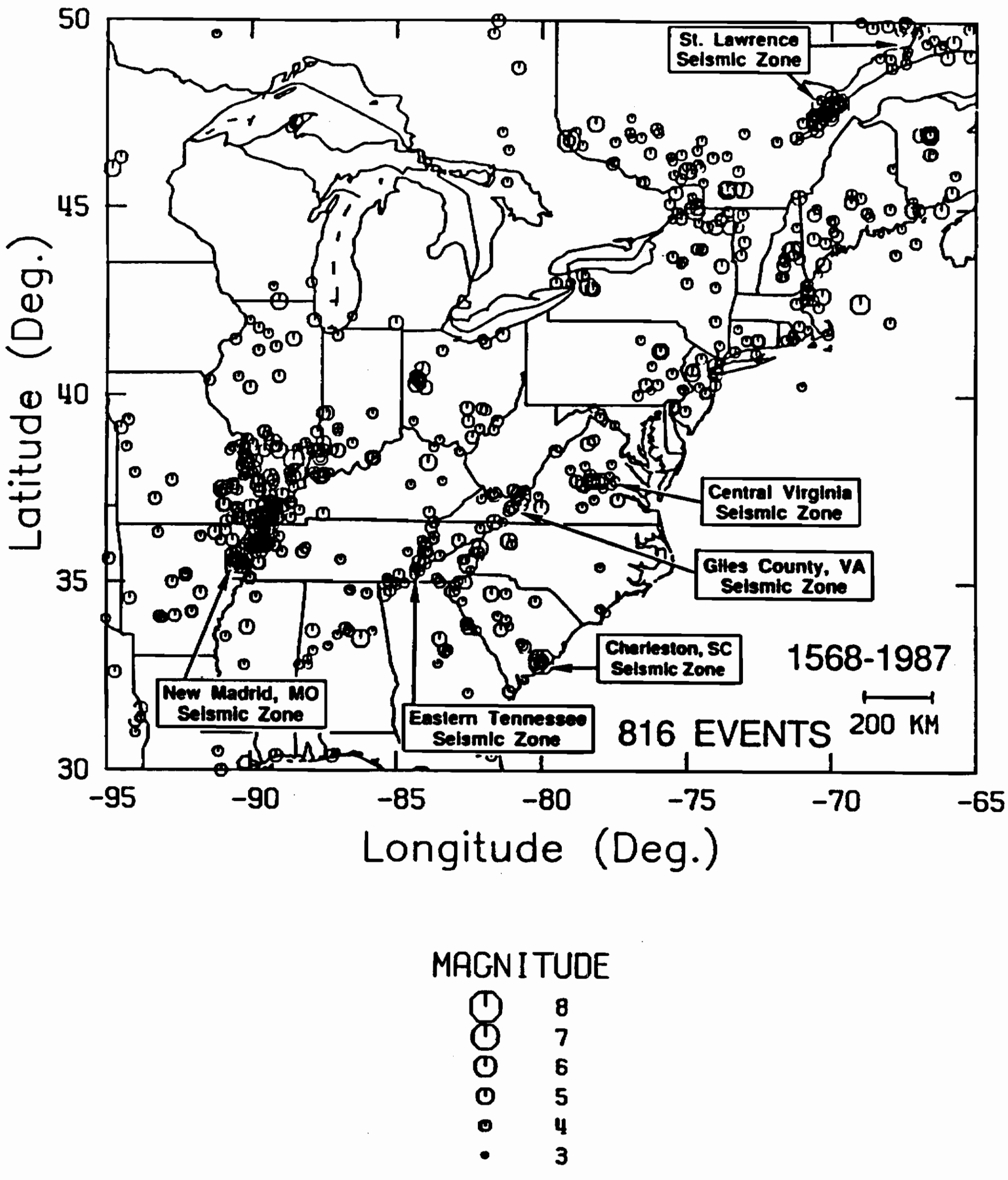

Figure 1. Seismicity of the Eastern North America: Intraplate seismicity (epicenters as circles) for the period 1568 - 1987. The labeled seismic zones have a spatial association with major river basins. Figure after Costain and Bollinger (1991).

The Charlevoix Seismic Zone

Structure and Seismicity

The Saint Lawrence valley has a long and complex geological history. Present day seismicity is occurring along ancestral normal faults that were either generated or reactivated by the opening of the proto-Atlantic Ocean (Iapetus, 600-700 MYA), and the reopening of the Atlantic Ocean (150-200 MYA) (Wilson, 1966 in Hasegawa, 1986). Most of the seismic activity of the St. Lawrence valley is concentrated into distinct clusters separated by aseismic areas, indicating that the several distinct seismic zones are not connected by a single fault system that is active along the entire valley (Figure 2; Lamontagne, 1987).

The Charlevoix Seismic Zone of the St. Lawrence valley is an intraplate cratonic seismic zone. The earthquake activity is confined to the Precambrian age rocks of the Grenville Province that crop out along the north shore of the St. Lawrence river. The south shore of the river consists of Paléozoic sediments of the Appalachian Province with 7 to 8 km thickness overlying the Precambrian basement. These Paleozoic sediments are separated from the Precambrian rocks by

Logan's Line (Figure 2); a contact that follows the north shore of the St. Lawrence river and dips at an average angle of 20° to the southeast (Rondot, 1972a; Leblanc and Buchbinder, 1977).

Three major fault systems, all trending NE to NNE and related to the major tectonic events mentioned earlier, occur in the Charlevoix seismic zone. The three episodes of faulting are the continental collision at the end of the Grenvillian Orogeny (1050-950 MYA), the opening of the Iapetus Ocean (600-700 MYA), and the Taconic Orogeny (450 MYA). Superposed on these three fault systems are faults concentric about Mount des Éboulements that are the result of a meteor impact (Rankin, 1975; Kumarapeli and Saull, 1966; Roy, 1978; as in Lamontagne, 1987). The impact structure is of Devonian age (350 MYA; Rondot, 1971) and has a diameter of 36 km with the central uplift located in the north shore of the St. Lawrence, at Mount des Éboulements (47.53°N 70.30°W; Rondot, 1968,1970) as shown in Figure 3.

Meteor craters worldwide are found to be seismically inactive, except for two locations; the Charlevoix region and the Vredefort structure in South Africa. Both of those locations exhibit the intersection of meteoric structures with rift systems; the St. Lawrence valley, a generally inactive rift system at the present, and the seismically active East African rift system (Solomon and Duxbury 1987). In the Charlevoix region, seismicity occurs mainly where the southeast half of the impact crater overlaps the St. Lawrence river, providing an impact crater - paleorift fault association. It has been suggested that the meteor impact may have weakened and reactivated the paleorift faults within the impact crater (Lamontagne, 1987; Anglin 1984; Leblanc and Buchbinder, 1977); it may have also increased the permeability of the paleorift faults allowing water from the river to effect pore pressure changes, silicate corrosion and chemical changes in fault gouge (Hasegawa, 1986). The distribution of hypocenters for shocks that occurred between 1977 and 1986 supports the postulate that the seismic activity occurs on faults formed prior to the impact structure and that there is no direct association between the patterns of seismicity and the crater faults (Buchbinder et al., 1988). However, the intersection of the crater faults and the paleorift faults may have indeed provided mechanically for the concentration of strain deformation eventually exhibited as the seismicity observed within the impact crater.

The Charlevoix seismic zone has been monitored by a local seismic network since 1977. Analysis of the network data shows that the Charlevoix region is under high compressional stresses that are reactivating ancient rift faults (Buchbinder et al., 1988). As proposed by Lamontagne (1987), the earthquakes are not necessarily occurring on only the paleorift fault surfaces. Analysis based on focal mechanisms inside the impact crater suggests that the microearthquakes occur on zones surrounding the rift faults (Lamontagne, 1987). The orientation of these zones is similar to the paleorift fault orientation, i.e. they strike parallel to the northeasterly trending St. Lawrence valley and dip steeply to the southeast (Anglin, 1984). Similar orientation was exhibited by the preferred nodal plane solution (strike N46°E, dip 76°SE) of the magnitude 5.0 event of August 19, 1979, the largest event recorded in the Charlevoix seismic zone since 1952 (Hasegawa and Wetmiller, 1980). The Charlevoix area has experienced some of the deepest earthquakes in eastern North America. The hypocenters range from 5 to 25 km depth and the corresponding focal mechanisms show no discernible relationship to depth for the entire zone (Lamontagne, 1987).

The Charlevoix Seismic Zone extends over an area roughly 90 by 35 km, between the Ile aux Coudres (47.20°N, 70.42°W) and Ile aux Lievres (47.90°N, 69.72°W), that can be bounded by a hexagon as shown in Figure 3. For purposes of comparison, the same analyses were applied to a four-sided "extended" zone that includes the Charlevoix Seismic Zone (Figure 3). Seismicity analysis of both zones did not yield appreciably different results, and thus, only the analysis of the Charlevoix seismic zone proper is presented herein. The earthquake catalog available (the Canadian Earthquake Epicentre File) is a nearly three and one-half century long data set obtained from the Geological Survey of Canada.

The Charlevoix region is the most seismically active zone in the Eastern North America. In the last 3.3 centuries it has shown persistent seismic activity with earthquakes up to magnitude 7.0. Furthermore, there is evidence of a much longer seismic activity in the Charlevoix region. A study of silt layers in organic-rich sediments in Lake Tadoussac, Charlevoix, suggest a 2300 year seismic history with four events of magnitude 7.5 or greater and eighteen events of magnitude 6 to 7, separated by intervals of time varying from 75 to 120 years (Doig, 1990). The Charlevoix Seismic Zone is obviously a hazardous zone with the potential for damaging earthquakes and it has been under extensive geophysical monitoring since 1974 (Buchbinder et al., 1988).

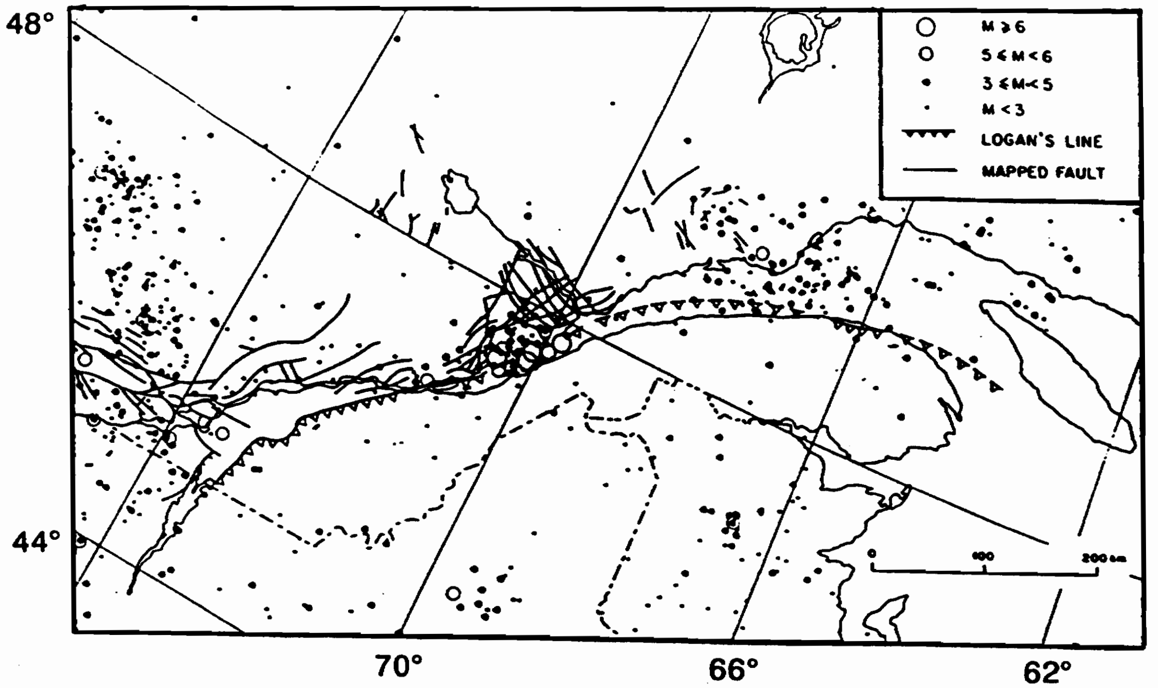

Figure 2. Seismicity and Faulting Along the St. Lawrence Valley: Epicenter map of the St. Lawrence Valley for the period 1663-1986, and major tectonic features along the Valley. The Charlevoix seismic zone is located approximately at 48°N, 70°W. Note the generally northeasterly trending of the major faults along the St. Lawrence Valley. Figure after Lamontagne (1987).

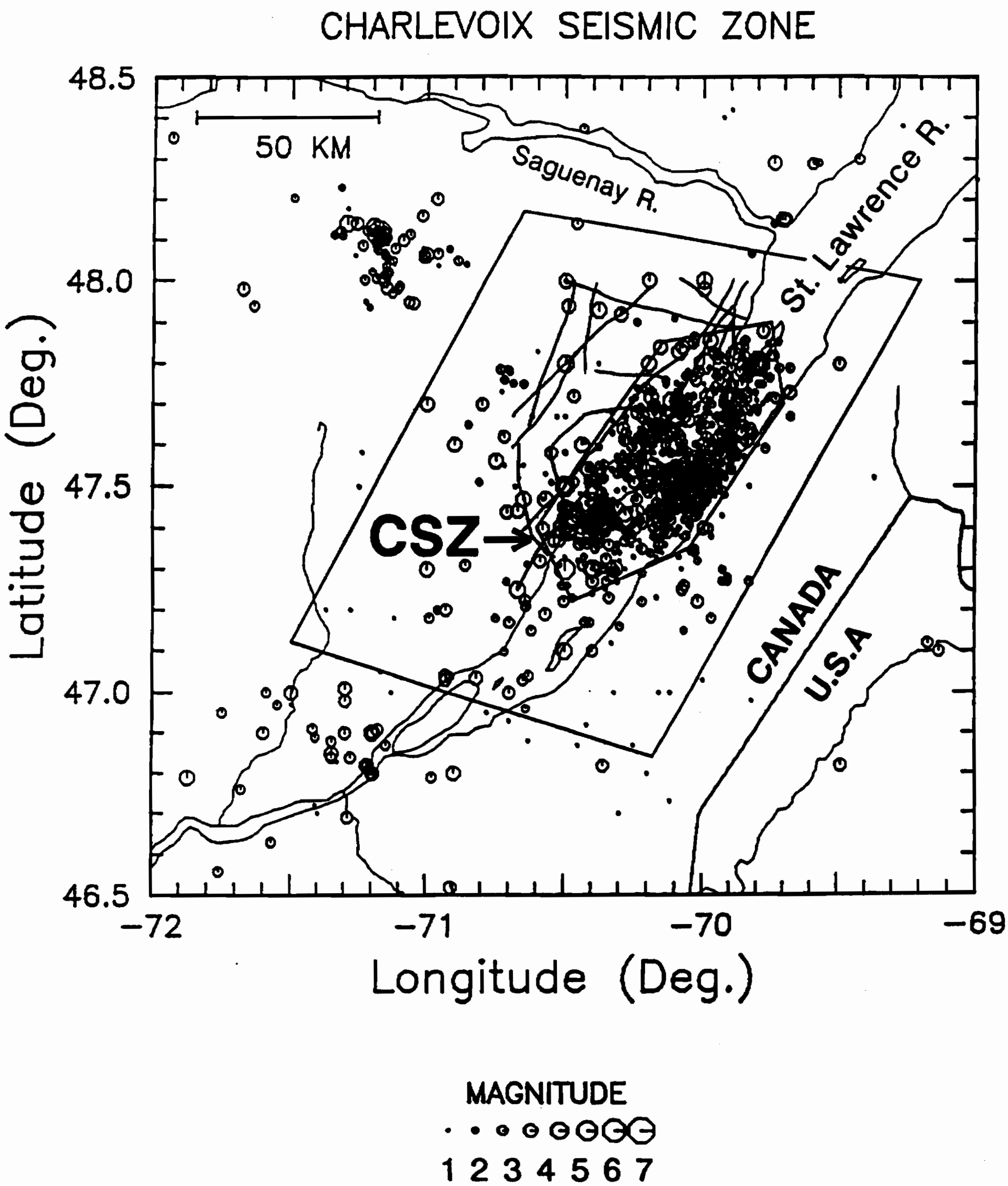

Figure 3. **The Charlevoix Seismic Zone - CSZ:** Epicenter map and faulting of the Charlevoix region along the St. Lawrence River. The Charlevoix seismic zone, with 1026 earthquakes for the period 1663-1990, extends over a hexagonal area roughly 90 by 35 km. The rectangular area encloses an auxiliary zone. Note the northeasterly trend of faulting in the seismic zone and the concentric faults associated with a meteor impact 350 MYA. The source of data is the Canadian Earthquake Epicentre File obtained from the Geological Survey of Canada. Fault positions were taken from Lamontagne (1987).

Cyclicities in the Seismicity

The interoccurence times of earthquake occurrences for a given region may be modeled as a Poisson process (Ang and Tang, 1975). In a recent study of earthquake recurrence models, Cornell and Winterstein (1988) concluded that if there are two or more faults at a site, "the combined hazard is better estimated by the Poisson model than is the hazard from any single feature". The multiple tectonic features of the Saint Lawrence valley at Charlevoix, as shown in Figure 3, make the Charlevoix seismic zone a viable candidate for the conventional Poissonian seismicity model. Note, however, that not all earthquake occurrences fit the Poisson model, as for example, the sequence of earthquakes in southern California studied by Gardner and Knopoff (1974). Other studies have shown that some observed seismic patterns can be described by deterministic chaos (Huang and Turcotte, 1990), and that earthquakes can also be viewed as self-organized critical phenomena (Ito and Matsuzaki, 1990). In this study, earthquake occurrences in the Charlevoix seismic zone are assumed to fit the conventional Poissonian model.

The source of seismicity data for the St. Lawrence Valley is the Canadian Earthquake Epicentre File, which was obtained from the Geological Survey of Canada. The earthquake catalog for the Charlevoix seismic zone is a 328-year record (1663-1990) of 1,026 events with magnitudes $0.0 \leq M \leq 7.0$. All catalog magnitudes for events prior to 1924 were determined from intensity measurements, i.e. damage and felt reports. Thus, some uncertainties are introduced for the earthquake parameters (magnitude and location) related to these older events. To minimize such uncertainties, and also to test the effects of an incomplete data set, subsets of the earthquake catalog excluding the older events will be considered in the analysis. For the purposes of this study a consistent measure of magnitude is needed. Therefore, body wave magnitudes (m_b) are employed that, for the older events, were determined from felt area reports and epicentral intensity (Sibol et al., 1987), as shown in Table 1. The discrepancy shown by the m_b estimate of the 1663 event is probably because of inaccurate felt area reports due to the scarcely populated areas in the 1700's. The earthquake catalog is judged to be incomplete for the time period before 1791, because there have been seven events reported for the two year period 1663 to 1665 and none for the following 124 years until 1791 (Figures 4 and 5). The smallest magnitude events reported in the period 1663-1970 (pre-network monitoring of the seismic zone) were $m_b = 2.4$. The data set analyzed in this study is subjectively reduced to a 200-year long record (1791-1990) with earthquake magnitudes $2.4 \leq m_b \leq 6.6$, for a total of 170 events. The average annual energy release is equivalent to one magnitude $m_b = 4.9$ earthquake per year.

To characterize the temporal release of the seismic energy, two measures of the seismic activity are considered in this study:

- The *strain factor* S, which is magnitude dependent, providing a physical parameter to relate directly to the seismic energy released in every seismic episode.

- The *number of earthquakes per unit time* N, which is magnitude independent, characterizing the temporal sequence of seismic energy release.

Strain Factor Analysis

The strain factor is a magnitude dependent measure of seismic energy release and is defined by the relationship:

$$E^{1/2} = 10^{(2.9 + 1.2m_b)} = S$$

where m_b is body wave magnitude of the event, E is the energy in ergs and S the strain factor in $(ergs)^{1/2}$ (Mento et al., 1986). This empirical relationship was derived from events of magnitudes $4.0 \leq m_b \leq 8.0$; however, it is assumed to be a valid expression for the range of magnitudes in the present analysis. Strain factor analysis was also employed by Mento (1986) and Setterquist (1989), to determine the temporal characteristics of the seismic energy release of the New Madrid and Central Virginia seismic zones, respectively.

The annual strain factor is calculated for the entire data set (1663 - 1990) and plotted in Figures 4 and 5. Note the significant energy release episodes occur about every 55 to 70 years. The cumulative strain factor versus time (Figure 6) has a typical stepped appearance, indicating periods of time for energy accumulation and for energy release.

The seismic energy release represented by the strain factor is analyzed for periodicities using Residual analysis and Fourier analysis (see e.g., Setterquist 1989).

Residual analysis is a standard statistical technique to search time series data for long term tendencies. For this study, residual strain was obtained by subtracting the least-squares fit line to the cumulative strain factor from the cumulative data. In Figure 7, the annual strain factor is cumulated for the years 1791 to 1990 and for $m_b \geq 2.4$ earthquakes. The cumulative strain factor is fit with a straight line that represents the average rates of annual earthquake energy release. The resulting residual annual strain factor (Figure 8) has a cyclical appearance, indicating three long term cycles: first cycle 1791 to 1860 (70 years), second cycle 1860 to 1925 (66 years), and a third unfinished cycle beginning in 1925. Note that the accumulated strain may be released in a single event, as in 1791 and 1925, or in more than one consecutive events, as in 1860 and 1870 when two major events were required to bring the energy release above the mean level (Figures 4,7 and 8). The effect of cumulation on the time series is equivalent to low pass filtering (division by $i\omega$), thus, the cumulated data tend to emphasize the longer periods.

Conventional **Fourier spectral analysis** was applied to the annual strain factor (S) using SPECTRA (SAS, 1985). The SPECTRA procedure estimates the spectral densities of a time series using a finite Fourier transform to obtain periodograms. The resulting periodogram of the strain factor (Figure 9) for the 200-year long data set, indicates a short term period of 13.4 years as well as a long term period occurring at 67 years. The strain factor periodogram peak with the largest amplitude corresponds to 13.4 years (Figure 9). It is however not a very dominant peak.

To examine the effects of an incomplete earthquake catalog (for the older events) in the cyclicities detected, two data subsets were also subjected to Fourier analysis with the following results.

- From 1830 to 1990, a 160-year long record indicated principal cyclicities of 13.3-year periods as well as 55-year long term periods.

- From 1900 to 1990, a 90-year long record indicated principal short term cyclicities of 13-year periods. This data set is not long enough to yield information about the longer term cyclicities.

Thus, the Fourier analysis of the annual strain factor indicates a principal short term cyclicity of approximately 13-14 years. The residual analysis of the annual strain factor, along with the Fourier analysis of the same data set, suggest a long term cyclical seismic energy release of 55 to 70 years.

Number of Earthquakes Per Unit Time Analysis

In the preceding analysis of cyclicities in the seismic energy release, the strain factor, which is a function of the magnitude of the earthquake, was considered. Lewis (1970), in a study of periodograms as a basis for estimation of cyclic trend components in a series, considers the events in the series, i.e. earthquakes, distinguishable only by where they occur in time. He defined a random variable, δ_t, which takes values 1 or 0 depending upon whether an event did or did not occur at time t. Also, a counting process (N) is defined as the number of events which have occurred in a time interval (k). Therefore, seismic energy release in the Charlevoix seismic zone can also be tested for cyclicities on the basis of the number of events (N) per time interval (k = 1 year). The magnitude of an event can be considered to be an independent random variable, needed only to assess the completeness of the catalog analyzed (Chapman 1990, personal communication).

The analysis employed to estimate cyclic components in the number of events time series is Fourier spectral analysis, as indicated by Lewis (1970). To ensure the completeness of the earthquake catalog over the entire length of the 200 year long data set, and furthermore to eliminate events associated with major earthquakes (foreshocks and aftershocks), a threshold magnitude m_b = 5.0 is assigned. The resulting data set consists of 8 events of magnitudes $m_b \geq 5.0$ for the 1791 to 1990 period, each with unit amplitude (Figure 10).

The **Fourier spectral analysis** of the number of events per year with $m_b \geq 5.0$ time series yields the periodogram shown in Figure 11, with the 13.4 year periodogram ordinate having the largest amplitude and the 67 year periodogram ordinate corresponding to the longest periodicity detected. To examine the effects of incomplete time series and also examine the stability of the number of events analysis with respect to the cyclicities observed, Fourier analysis was applied to data sets of varying threshold magnitudes i.e. data sets with varying number of events, and to data sets with events deleted and/or added at random, with the following results.

- For magnitudes $m_b \geq 4.5$, the resulting data set has 12 events for the period 1791-1990, and yields the largest periodogram ordinate at 13.4 year periods and the longest periodicity at 67 years.

- For magnitudes $m_b \geq 5.5$, the resulting data set has 6 events for the period 1791-1990, and also yields the largest periodogram ordinate at 13.4 year periods and the longest periodicity at 67 years.

- For magnitudes $m_b \geq 5.0$, as in Figure 10, but with one event deleted at a time, the largest periodogram ordinate also occurs at 13.4 years, as expected.

- For the time series of Figure 10, deleting two or more events and/or adding one or more events at random, yields periodogram ordinates with amplitudes larger than the one at 13.4 years. That is, the periodogram changes. It should be noted that if the deleted and/or added events fall at the right times, the resulting periodogram shows the largest ordinate at 13.4 years, as expected.

Thus, the Fourier analysis of the number of earthquakes per year time series indicates cyclic trend components with the largest periodogram ordinate corresponding to short term cyclicities of 13.4 years along with long term cycles of 67 year periods.

Periodogram Ordinate Significance Tests

The periodograms of annual strain factor and number of events per year (Figures 9 and 11) are used to determine periodicities in the seismicity time series. The periodogram ordinates with the largest amplitude correspond to periods of 13.4 years, suggesting cyclicities present in the time series at that period. However, is the 13.4 year periodogram ordinate statistically significant? Fisher

(1929) derived a test statistic, g, for the significance of the amplitude of the largest periodogram ordinate **max(I_p)** in a sample of **m** periodogram ordinates. The SPECTRA (SAS, 1985) procedure prints the alternative version of Fisher's test statistic, κ (kappa) as determined by Fuller (1976), where κ is related to g by the expression:

$$\kappa = mg$$

and

$$\kappa = \frac{\max(I_p)}{\frac{1}{m}\sum_{p=1}^{m}(I_p)}$$

Under the null hypothesis that a time series is white noise (i.e. no periodogram ordinates are significantly larger than any other), the κ values calculated by the SAS SPECTRA procedure for the 13.4 year periodogram ordinate and for m = 100, are $\kappa = 6.74$ for the number of events per year periodogram, and $\kappa = 2.4$ for the strain factor periodogram. Table 7.1.2 in Fuller (1976) gives percentage points for κ for given values of m. For m = 100, κ is 6.71, 7.38 and 8.88 at the corresponding 10%, 5% and 1% levels of significance (Fuller, 1976). Therefore, because the calculated κ for N (6.74) is larger than 6.71 of Fuller's table, the null hypothesis is rejected at the 10% level of significance, i.e. there is a 90% probability that the 13.4 year periodogram ordinate is larger than any other in the number of events per year periodogram. Although this statistical test does not yield conclusive results ,i.e., a 99% probability, the 90% probability obtained is judged to be acceptable for developing conclusions in this analysis. The calculated κ for S (2.4) is much smaller than 6.71, thus the 13.4 year strain factor periodogram ordinate fails to reject the null hypothesis at statistically accepted levels of significance. Thus, according to Fisher's κ test, the strain factor time series meets the criterion of white noise.

To test the sensitivity of the spectral analysis and Fisher's κ test to the binning of time series, and, consequently, to the number of periodogram ordinates m, the same analysis is applied to the monthly strain factor, whose periodogram is shown in Figure 12, with m = 1323, and to the number of events every two years, whose periodogram is shown in Figure 13, with m = 50. Note that the periodogram of monthly strain factor does not indicate any dominant peaks, whereas the periodogram of number of earthquakes every two years indicates consistent periodicity results with the earlier analyses, showing short term cyclicities corresponding to 13.4 years along with longer cyclicities of 67 year periods. Fisher's κ test of both data sets yields consistent statistical results with the earlier analyses. The number of events every two years 13.4 year periodogram ordinate tested significant at the 10% level of significance, with a calculated $\kappa = 6.3$ compared to table 7.1.2 (Fuller, 1976) with κ values of 5.9, 6.6 and 8.0 at the corresponding 10%, 5% and 1% levels of significance. The monthly strain factor failed to reject the null hypothesis at the 10% level of significance, with a calculated $\kappa = 2.6$ compared to a value of 9.1 from table 7.2.1 (Fuller, 1976); thus, as before, the strain factor time series tested as white noise.

Fourier spectral analyses on the two measures of seismic energy release, the strain factor and the number of events per unit time, yielded common short term cyclicities of approximately 13-14 year periods along with long term cyclicities of 55 to 70 year periods. Varying the data set length, threshold magnitude, and binning of data, yielded same cyclicities indicating a stability of the analysis procedure and completeness of the data set analyzed. Fisher's periodogram ordinate test applied to the spectral analysis results, showed that the 13.4 periodogram ordinate of the N analysis is significant at the 10% level of significance, whereas the 13.4 year periodogram ordinate of the S analysis failed to test significant. Fisher's test also showed stability with respect to binning the data. Although the strain factor 13.4 periodogram ordinate failed to test statistically significant, it is in agreement with the statistically significant number of earthquakes 13.4 year periodogram ordinate. Therefore, the strain factor does reflect some of the temporal characteristics of the seismicity and is therefore utilized in this study along with the number of earthquakes per unit time.

Residual analysis of the annual strain factor shows variation about the mean with cyclic, but not periodic, behavior. The cycles indicated by the residual strain factor are approximately 65 to

70 years long, and are in general agreement with the long term cyclicities suggested by the spectral analysis of both seismicity time series.

Studies in the seismic energy release (the strain factor) of other intraplate seismic zones in the eastern United States, indicated the following cyclic behavior of seismicity: The New Madrid seismic zone (NMSZ) yielded a cyclical strain factor with period of 30 - 35 years, for a 70-year long record with earthquakes of $m_b \leq 5.5$ and an annual energy release equivalent to one magnitude $m_b = 4.5$ earthquake per year (Mento and others, 1986). The Central Virginia seismic zone (CVA) yielded 20 $\pm$ 2-year periods of seismic energy release, for an 85-year long record with events of $2.4 \leq m_b \leq 4.2$ equivalent to one magnitude $m_b = 2.5$ earthquake per year (Setterquist and Sibol, 1988). A plot of the cumulative strain factor of the Charlevoix (CSZ), New Madrid, Central Virginia, and Giles County (GCO) seismic zones (Figure 14) shows that the Charlevoix seismic zone has been the most seismically active zone in the eastern North America in the past one and a half centuries.

Table 1. **Canadian Catalog Magnitudes vs Calculated Body Wave Magnitudes**

Year	Canadian Cat.	m_b Catalog
1663	7.0 M_L	5.8 m_b
1665	5.5 M_L	5.2 m_b
1791	6.0 M_L	5.8 m_b
1860	6.0 M_L	6.1 m_b
1870	6.5 M_L	6.2 m_b
1924	5.5 m_n	5.5 m_b
1925	7.0 M_S	6.6 m_b
1939	5.6 m_n	5.6 m_b

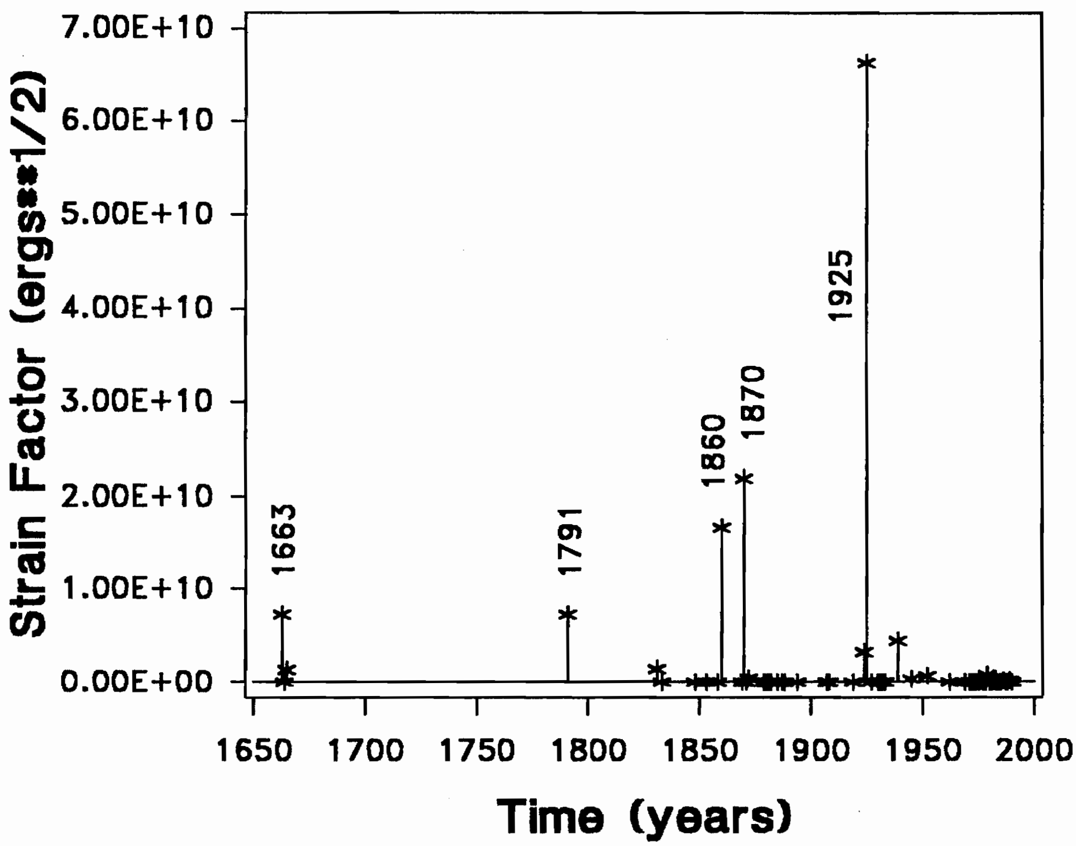

Figure 4. Strain Release in the Charlevoix Seismic Zone, 1663-1990: Annual strain factor (S) in the Charlevoix region for a total of 1026 events. Note the energy release episodes occur about every 55 to 70 years: $E^{1/2} = 10^{(2.9 + 1.2m_b)} = S$.

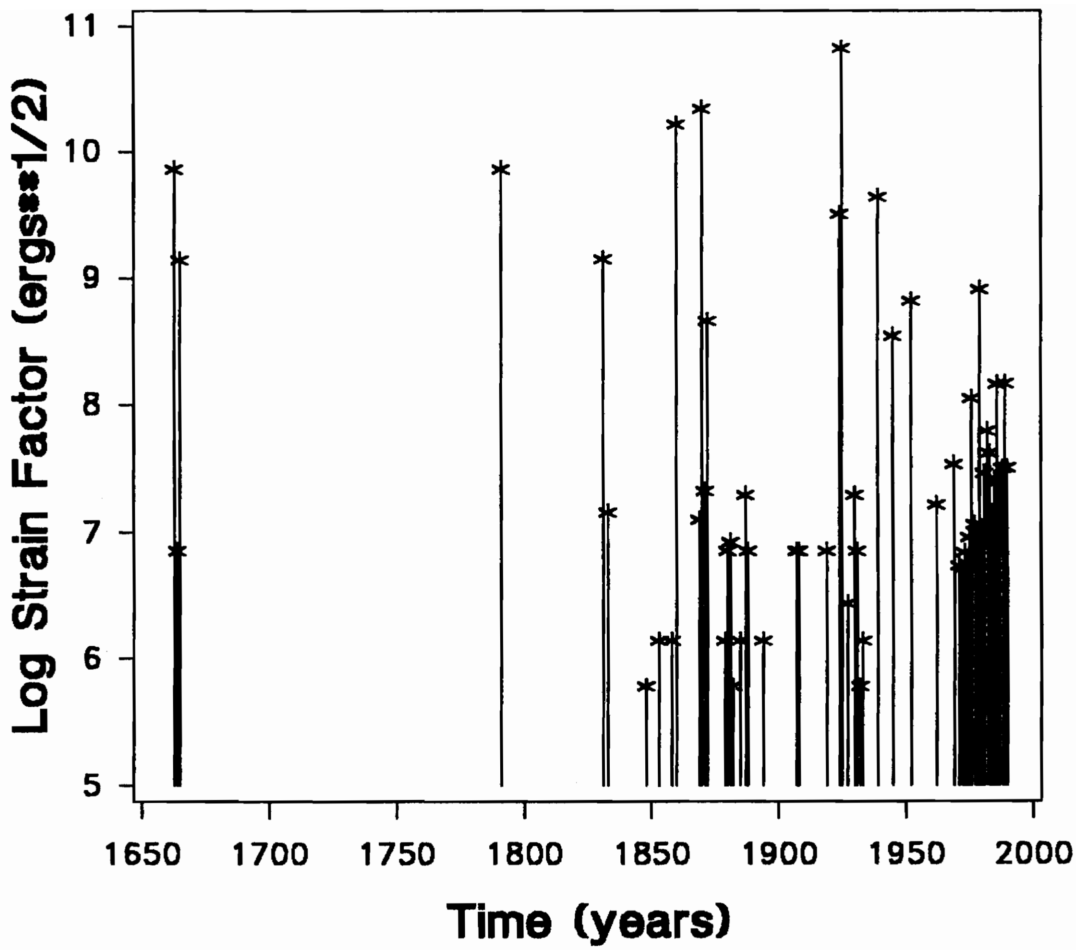

Figure 5. **Logarithm of Strain Release in the Charlevoix Seismic Zone, 1663-1990:** Logarithm of annual strain factor in the Charlevoix region for a total of 1026 events. Another representation of the data of Figure 4, showing relative amplitudes for all data analyzed.

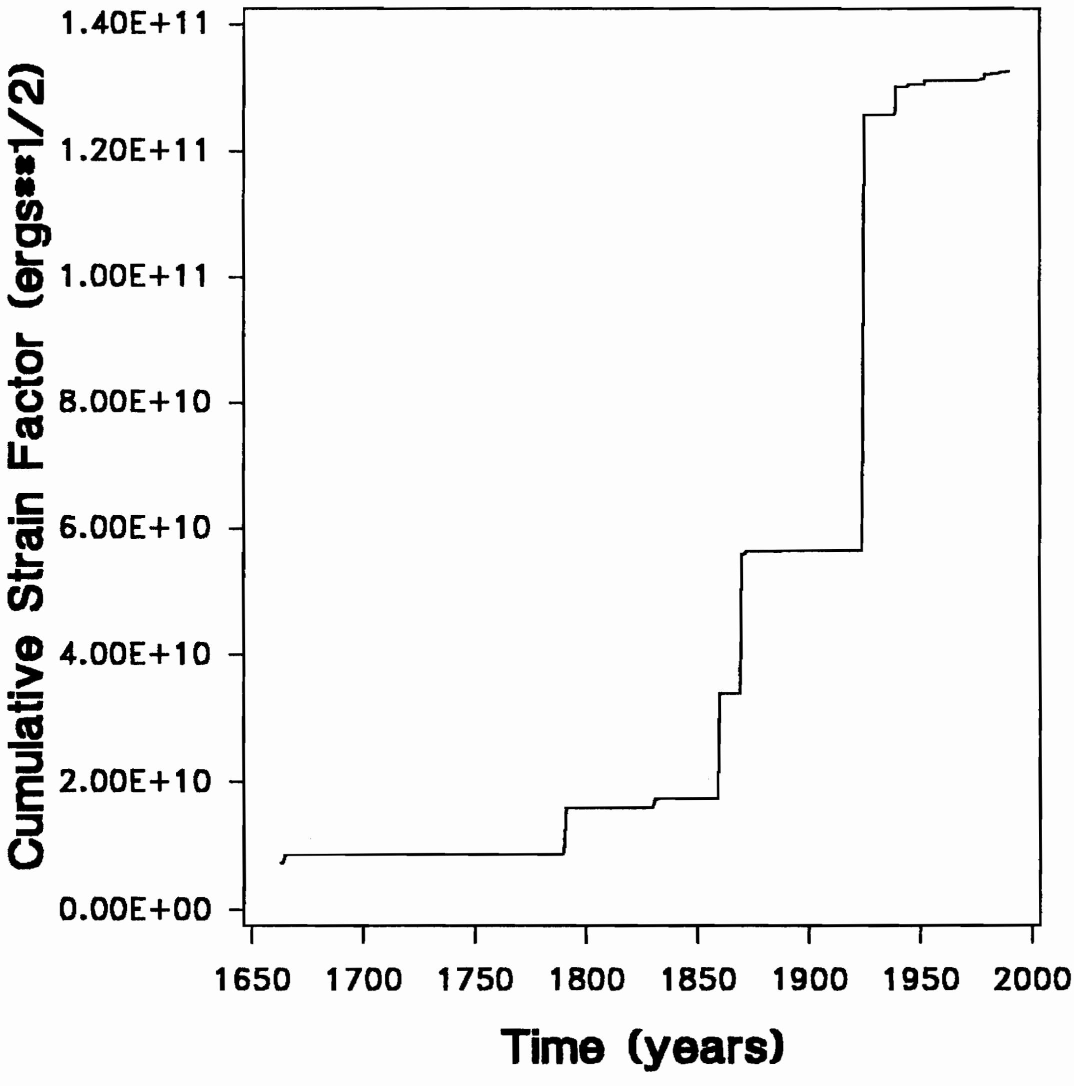

Figure 6. Cumulative Strain Factor, 1663-1990: The stain factor is cumulated over time for the period 1663 to 1990. The stepped appearance of the cumulative strain factor indicates periods of seismic energy accumulation and release.

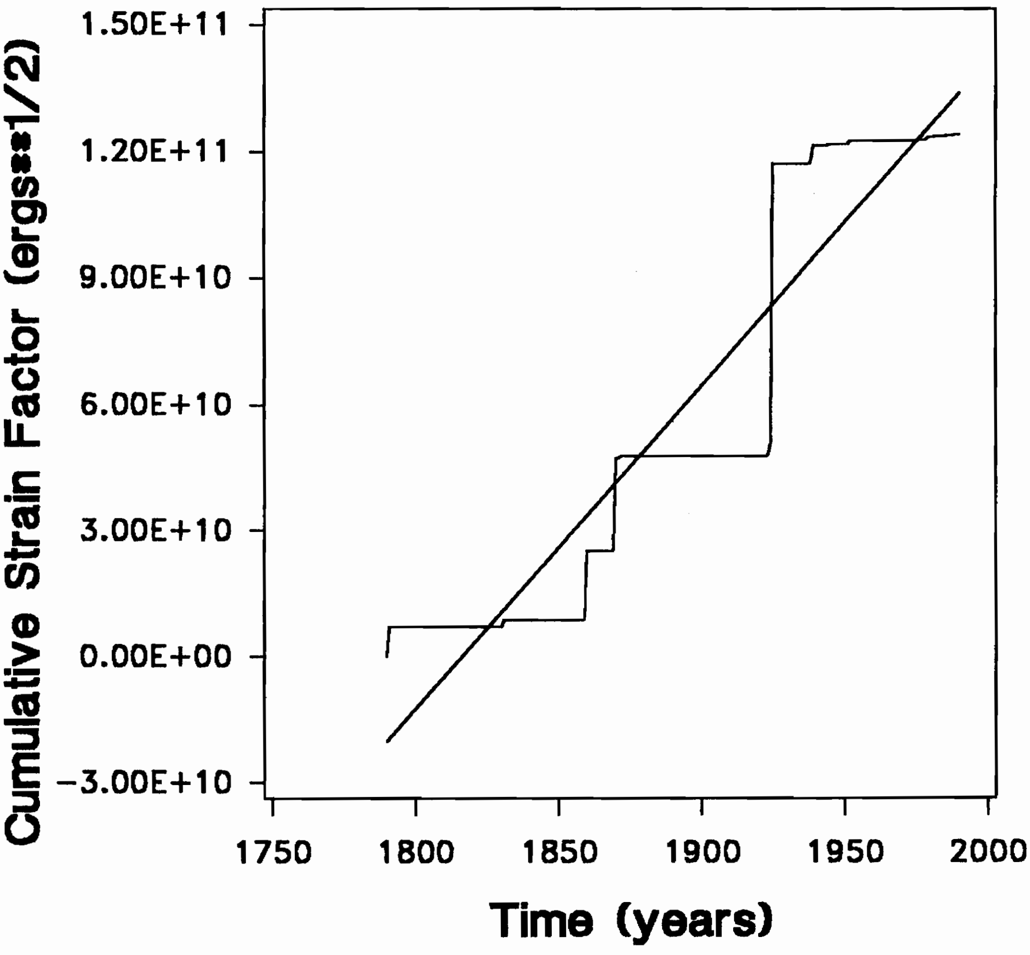

Figure 7. Cumulative Annual Strain Factor and Straight Line Fit, 1791-1990: The annual strain factor is cumulated for the 200 year long period data set with a total of 170 earthquakes. A straight line is fit to the cumulative S by least squares linear regression, representing the average annual energy release.

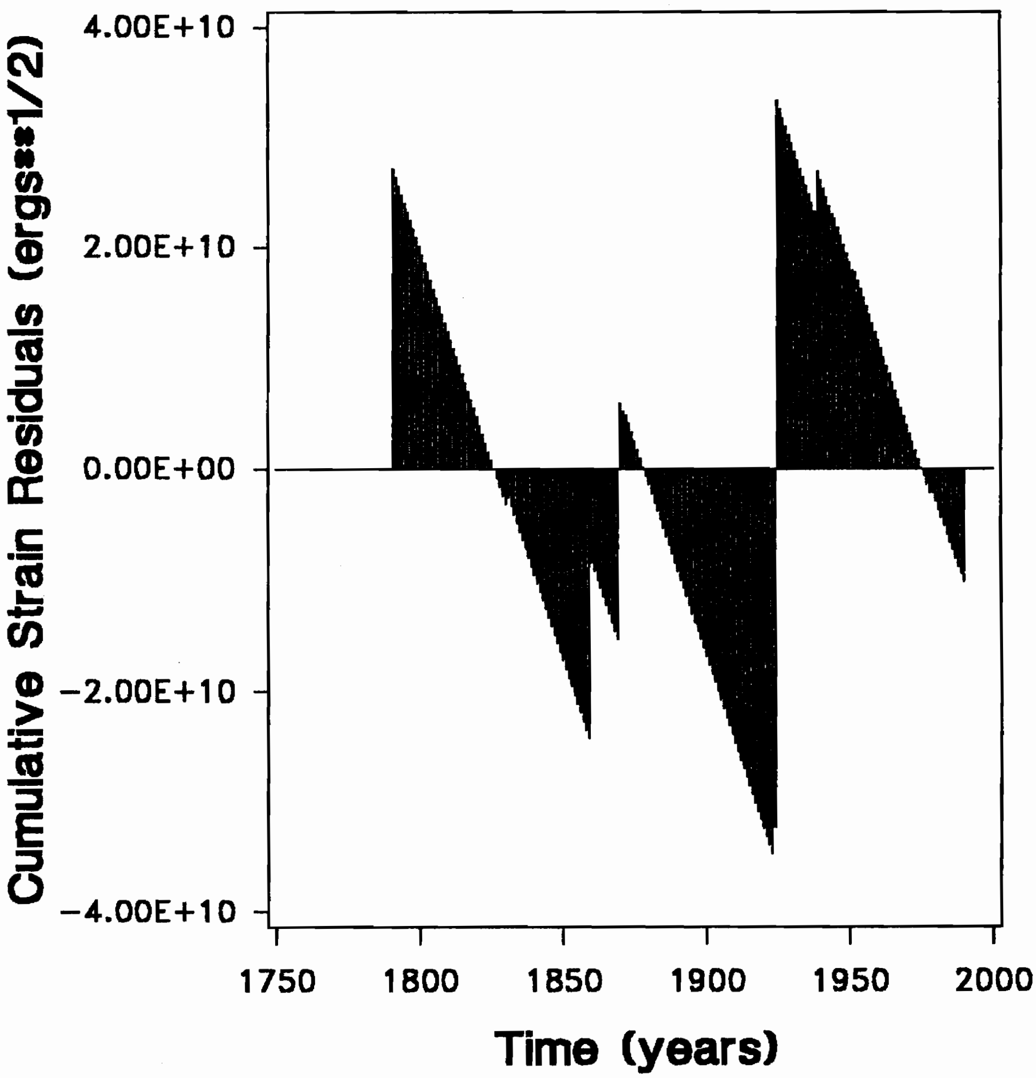

Figure 8. **Residual Annual Strain Factor, 1791-1990:** Residual strain factor obtained by subtracting the least-squares fit from the cumulative S. Note the cyclical appearance of residual S, with long term cycles of 65 to 70 years.

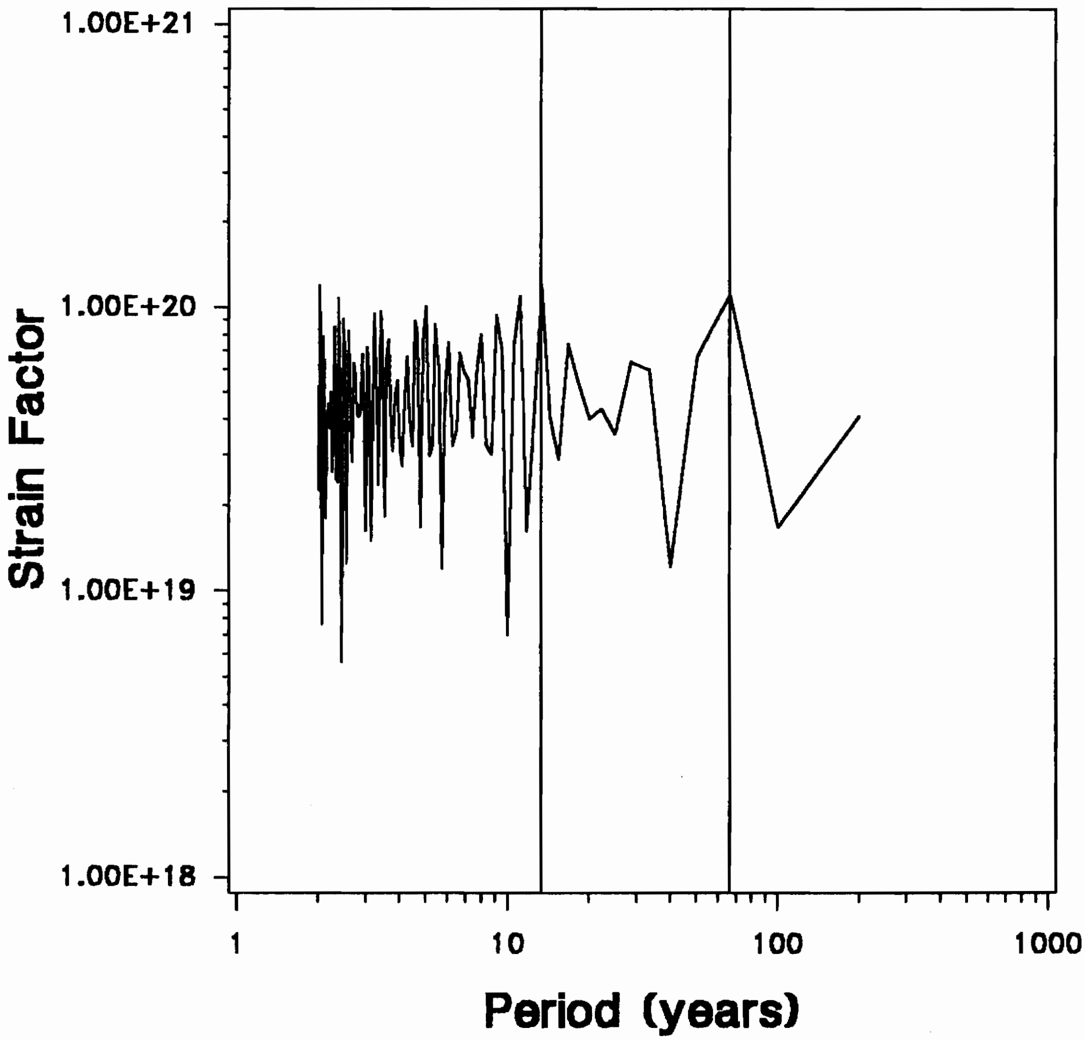

Figure 9. Periodogram of the Annual Strain Factor: The periodogram ordinate with the largest amplitude corresponds to 13.4 year periods and the long term peak corresponds to 67 years. Reference lines correspond to 13.4 and 67 years.

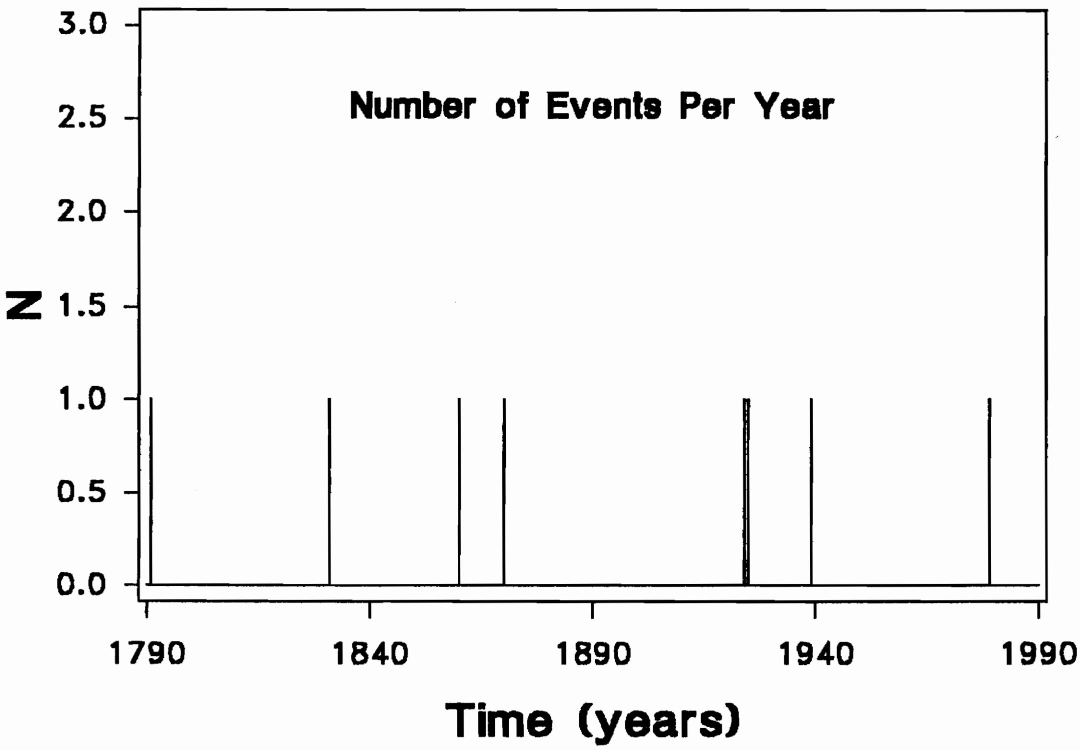

Figure 10. Number of Earthquakes Per Unit Time: Number of events (N) per year time series, at the Charlevoix seismic zone with magnitudes $m_b \geq 5.0$ for the period 1791 to 1990.

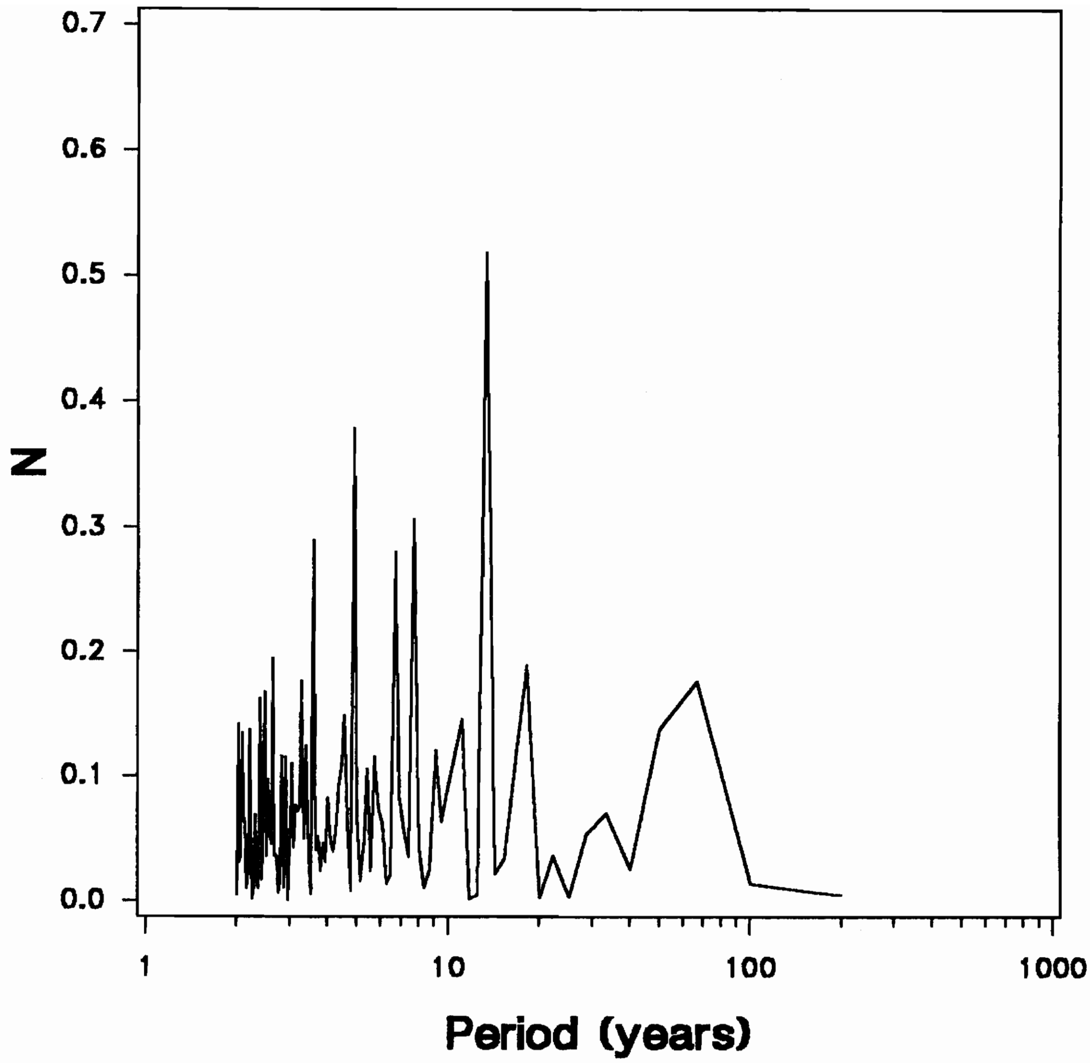

Figure 11. **Periodogram of Number of Earthquakes Per Year:** Periodogram of the number of earthquakes per year at the Charlevoix Seismic Zone with $m_b \geq 5.0$ for the period 1791 to 1990 with number of periodogram ordinates m = 100. The periodogram ordinate with the largest amplitude corresponds to 13.4 years.

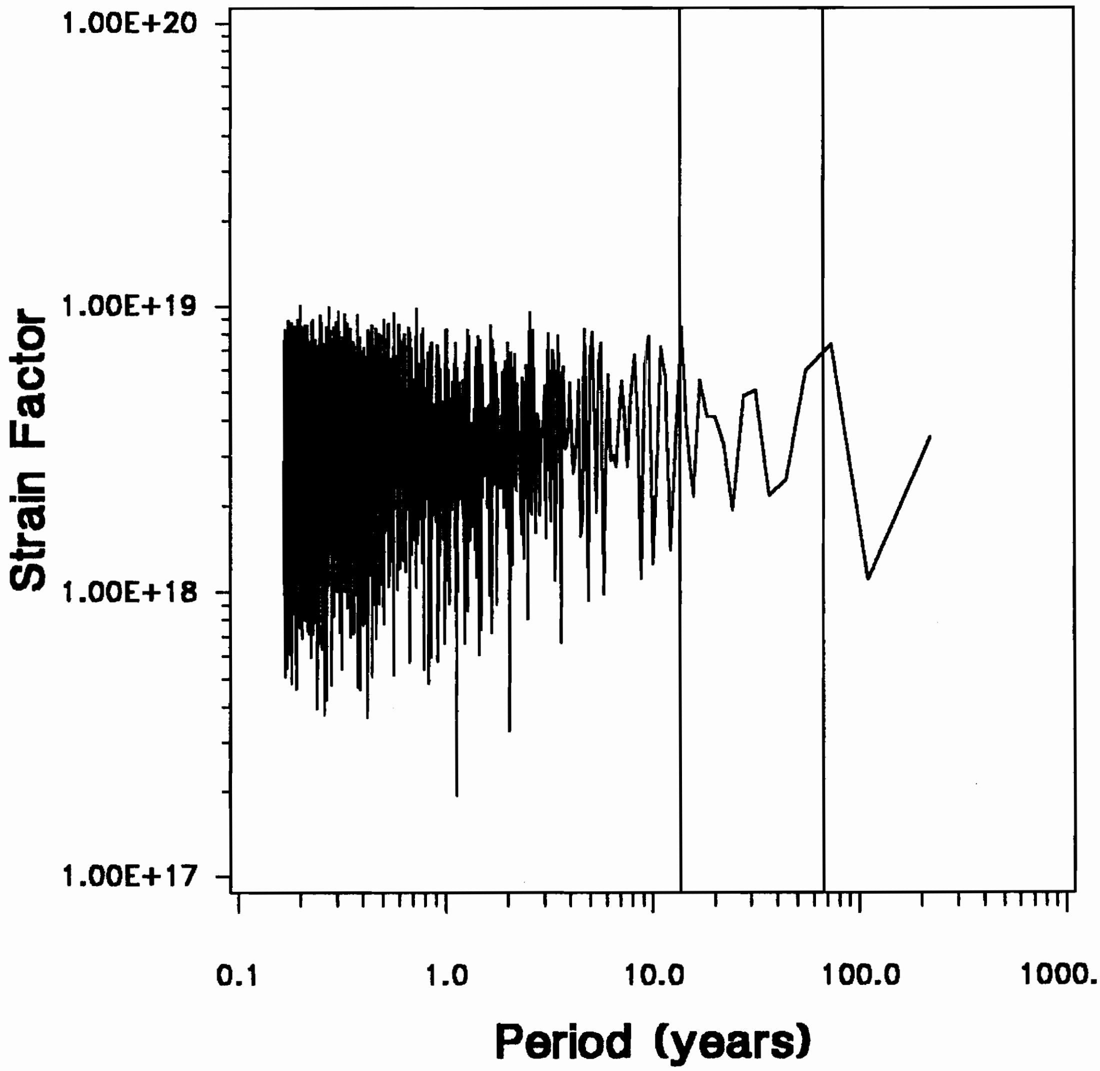

Figure 12. Periodogram of the Monthly Strain Factor, 1791-1990: Periodogram of the Monthly Strain Factor for the period 1791-1990, with m = 1323. Note that the appearance of the periodogram is as of white noise, i.e. no periodogram ordinate appears to be considerably larger than any other. Reference lines correspond to 13.4 and 67 years.

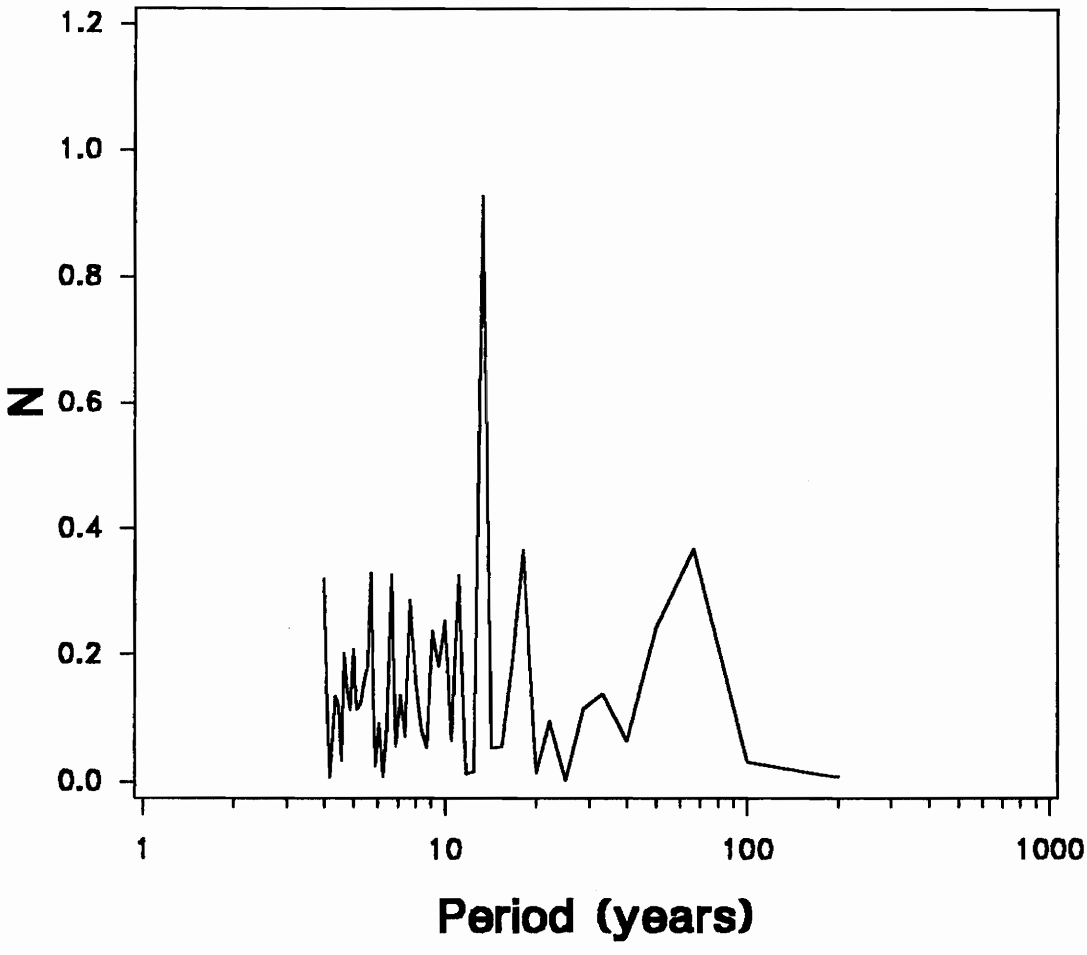

Figure 13. Periodogram of Number of Earthquakes Every Two Years: Periodogram of the number of events every two years at the Charlevoix Seismic Zone with $m_b \geq 5.0$ for the 1791 to 1990 period with m = 50. Similarly to the earlier analyses, the largest periodogram ordinate corresponds to 13.4 years, and the longest period ordinate to 67 years.

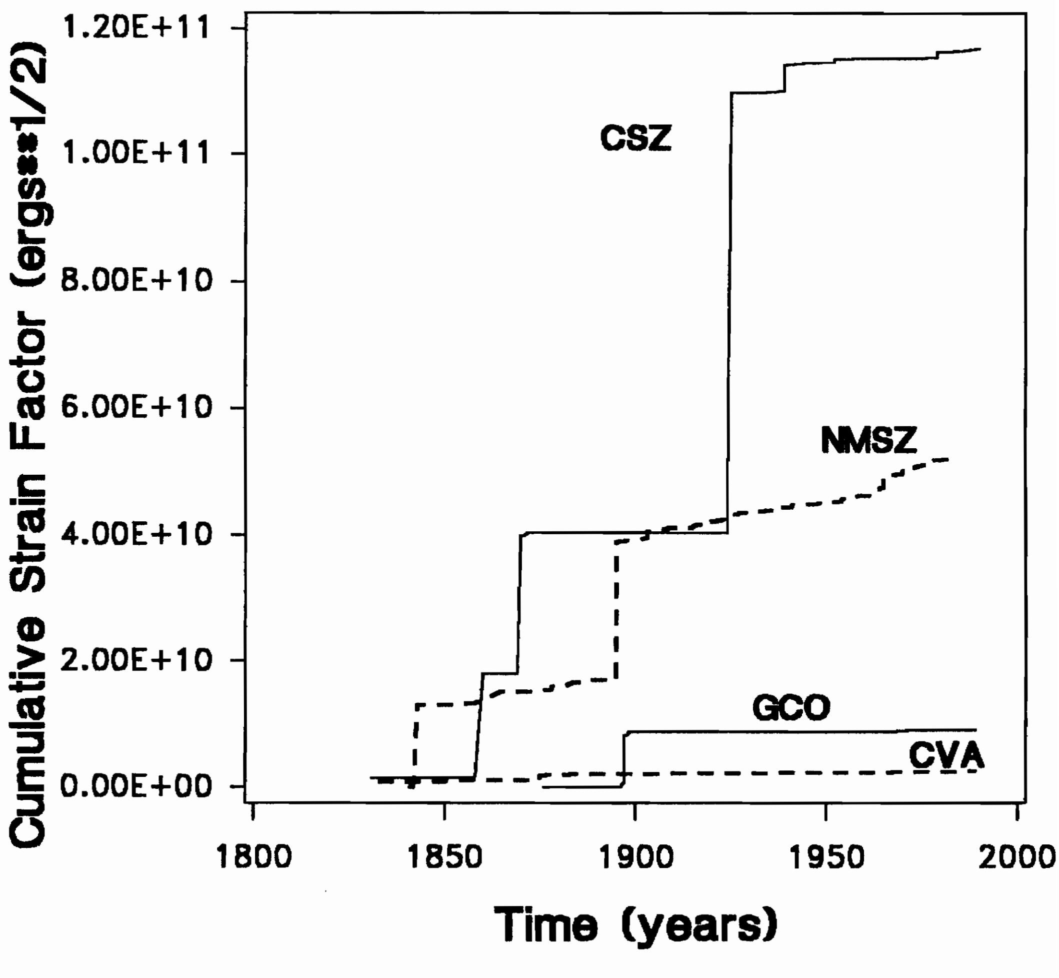

Figure 14. Comparison of Cumulative Strain: Comparison of cumulative strain among CSZ (Charlevoix, Canada), NMSZ (New Madrid, MO), CVA (Central Virginia) and GCO (Giles county, VA) seismic zones. In the past one and a half centuries, the Charlevoix seismic zone has been the most seismically active region in the eastern North America.

Temporal Characteristics of Water Levels in the St. Lawrence River

The Hydroseismicity hypothesis considers water table fluctuations as the source of pore pressure pulses diffused to hypocentral depths in the crust. To characterize the temporal characteristics of water table fluctuations in the St. Lawrence valley, and consequently in the Charlevoix region, the temporal behavior of water level fluctuations in the St. Lawrence river is analyzed.

The hydrometric data analyzed were obtained from the Water Survey of Canada and consist of:

- A 70-year long record of daily water levels (1919 - 1988) for the station 02OA040, on the surface of the St. Lawrence river at Lachine, 340 km southwest of the seismic zone.

- A 14-year long record of monthly water levels (1964 - 1977) for the station 02PA005, on the surface of the St. Lawrence river at Batiscan, 180 km southwest of the seismic zone.

- A 34-year long record of daily streamflow (1955 - 1988) for the station 02OA016, on the St. Lawrence at Lasalle, 340 km southwest of the seismic zone.

Thus, the hydrometric data sets available for analysis come from stations located 180 to 340 km upstream from the Charlevoix seismic zone in the St. Lawrence river (Figure 15). Temporal analysis between monthly water levels at stations 02OA040 (340 km SW of the seismic zone) and 02PA005 (180 km SW of the seismic zone and 160 km NE of 02OA040) indicate synchronous water level fluctuations in the St. Lawrence river (see Appendix A). Therefore, it is assumed that the 70-year long water level record of station 02OA040 is representative of the temporal water table fluctuations in the St. Lawrence valley, and consequently in the Charlevoix region.

Over the 70-year long record of daily water levels for the station 02OA040, a total of 117 days of water level data were missing, corresponding to 0.5% of the entire data set. The missing values were estimated using a linear approximation for missing intervals up to 3 days, and a cubic spline fit approximation for missing intervals from 4 to 8 days. From the daily water levels, monthly average water levels were calculated for the 70-year observations of station 02OA040, and are plotted in Figure 16.

To characterize the temporal behavior of the water table fluctuations in the St. Lawrence valley, the monthly water level data set of station 02OA040 is analyzed. It should be acknowledged that in the St. Lawrence river at the Charlevoix region there are some tidal effects present, but they are not directly considered in this analysis. The focus of this analysis is in the water table fluctuations of the St. Lawrence river basin (presumably represented by the St. Lawrence river water level fluctuations in the Montreal area) and not only in the river's level fluctuations in the Charlevoix region. Costain and Bollinger (1991) considered the monthly streamflow of the James river in Central Virginia as a non-linear measure of the water table fluctuations. In the present study, the water levels are to be analyzed, rather than the flow volume, because they are the longest time series available, 70 years long. As shown in Appendix B, there is an approximately linear relationship between water levels and stream flow in the St. Lawrence river, and, thus, they can be expected to exhibit similar temporal behaviors.

Water Level Analysis

Residual Analysis and *Fourier Spectral Analysis* as discussed earlier for the seismicity time series are also applied to the monthly water level data set.

The **monthly water level residuals** for station 02OA040 show a long term cyclicity of approximately 70 to possibly 80 years (Figure 17). Note that a full 80 year cycle is not present, however, there is a full half-cycle present (1936 to 1976) and two quarter-cycles, one at the beginning (1919 to 1936) and one at the end (1976 to 1988) of the time series. As previously discussed, the residual analysis emphasizes any long term cyclicities present in a time series. In the case of the 70-year long monthly water level data set, it is not certain whether the 70 - 80 year long periodicity implied is an actual one, because the time series is not long enough for a complete cycle. However, quarter cycles of approximately 20-year long occur throughout the time series.

Conventional **Fourier spectral analysis** is used to determine the presence of short term periodicities in the monthly water level data set. It is expected that the periodogram of the water levels will be dominated by the 1.0 year ordinate, corresponding to the seasonal precipitation cycle. However, in the study of Hydroseismicity we are primarily interested in periodicities greater than 1 year because the longer periods would more efficiently diffuse pore pressure changes to hypocentral depths. Therefore, the statistical significance of the second and possibly third and fourth largest periodogram ordinates needs to be determined.

As reviewed earlier, Fisher's test deals with the largest periodogram ordinate. However, Priestley (1981) gives the distribution of the ratio of the r-th largest periodogram ordinate to the sum of the periodogram ordinates under the null hypothesis that the time series is Gaussian, i.e. a normally distributed, purely random process (Grenander and Rosenblatt, 1957; as in Priestley 1981). Thus, to apply the Grenander-Rosenblatt method, the monthly water level time series must be transformed to a normal distribution. The CAPABILITY procedure (SAS, 1989) performs statistical tests to determine the distribution of a population. Under the null hypothesis that the monthly water level data has a Weibull distribution, SAS yielded a p-value of 0.31. Thus, at the 10% level of significance, i.e $\alpha = 0.10$, there is sufficient evidence to accept the null hypothesis, since $\alpha = 0.10 < p = 0.31$ (Figure 18). Note that p and α correspond to fractional areas under the curve, with the total area under the curve equal to 1.0. The null hypothesis was rejected at the normal, lognormal, beta and gamma distribution tests. Therefore, the monthly water levels at the St. Lawrence river are fit by a Weibull distribution. Box and Cox (1964) developed a general power transformation useful in situations where the original data are not normally distributed. After applying their transformation $z = y^{\lambda}$ to the monthly water level data (y), where λ was determined by trial and error to be equal to -1.800, the transformed water levels (z) were found to be normally distributed at the 10% level of significance ($\alpha = 0.10$) with a p-value$=0.59$ (Figure 19).

Fourier spectral analysis is applied to the transformed monthly water levels (z) using SPECTRA (SAS, 1985), and the resulting periodogram is shown in Figure 20. As expected, the largest periodogram ordinate corresponds to the seasonal water cycle of one year, however, the second largest periodogram ordinate corresponds to a period of 70 years. Because of the short length of the water level data set (70 years), periodogram ordinates at periods greater than 35 years cannot correspond to real periodic components in the time series. Furthermore, the periodogram ordinates corresponding to larger periods might appear to have large amplitudes because of the trend of the periodogram of increasing amplitudes with increasing period. To reduce the increasing trend of the periodogram of Figure 20 at the longer periods, a long period trend is subtracted out of the water level time series. As shown in Figure 21, a least-squares straight line is fit to the time series of monthly water levels and the detrended time series is plotted in Figure 22. The detrended time series is transformed to a normal distribution with p-value$=0.3$, using the Box and Cox transformation with $\lambda = 0.54$. The periodogram of the detrended water level time series is shown in Figure 23 with the largest periodogram ordinates (in decreasing amplitude order) corresponding to 1.0, 23.3, 14.0 and 7.8 year periods.

Periodogram Ordinate Significance Tests

The Grenander-Rosenblatt method is used to determine the statistical significance of the multiple largest periodogram ordinates of Figure 23. The results are shown in Table 2, in decreasing order of statistical significance, i.e. in decreasing κ value. The percent probability of the existence of a larger periodogram ordinate than the one tested is shown in the (% Probability) column. It should be noted that when computing κ and probability values of the second, third etc. largest periodogram ordinates, the ones that have already been tested, i.e. the first, second etc., are removed from the ratio. According to the results of the test (equation 6.1.73, Priestley 1981), there exists less than 0.01% probability for the existence of a larger periodogram ordinate when the 1.0, 23.3, 14.0 and 7.7 year periodogram ordinates are tested.

The sensitivity of the analysis procedure to the binning of the time series and consequently to the number of the periodogram ordinates was examined at station 02OA40. Selecting a bin of 1 year eliminates the 1-year seasonal peak, and thus, the several largest periodogram ordinates can be tested using the Grenander-Rosenblatt method (equation 6.1.73). The largest periodogram ordinate can also be tested using Fisher's κ test, as discussed in the seismicity analysis. Annual water levels fitted with a straight line by the least squares method are shown in Figure 24. The detrended annual water levels are analyzed similar to the detrended monthly water levels. Under the null hypothesis that the annual water level data is normally distributed, the CAPABILITY procedure yielded a p-value of $0.3 > \alpha = 0.10$, which indicates that the population is normally distributed. Fourier spectral analysis of the detrended annual water levels yielded consistent periodicity results with the earlier analysis, and its periodogram is shown in Figure 25, with the largest periodogram ordinate occurring at 23.3 years. The results of the Grenander Rosenblatt test are summarized in Table 3. According to the test, there is a 0.03% probability for the existence of a larger periodogram ordinate when the 23.3 year periodogram ordinate is tested. Fisher's κ test, also yielded a significant 23.3 year periodogram peak at the 1% level of significance, with a calculated

$\kappa = 9.93$ compared to table 7.1.2 (Fuller, 1976) with κ values of 5.6, 6.2 and 7.6 at the corresponding 10%, 5% and 1% levels of significance. Thus, the Grenander-Rosenblatt method is in agreement with Fisher's κ test, as expected. Although the κ and p-values of Table 3 are not as strong statistically as the corresponding values of Table 2, they do indicate the existence of the same dominant periodic components (23.3, 14.0 and 7.8) in the average monthly and annual water level time series.

Fourier spectral analysis of the average monthly water levels at station 02OA040 yielded a dominant cyclicity of 23.3 year periods, along with shorter cyclicities of 14 and 7.8 year periods. Average annual water levels also yielded cyclicities of 23.3, 14.0 and 7.8 years, indicating stability of the analysis procedure. The Grenander-Rosenblatt statistical test on the monthly and annual water level periodograms, indicated the 23.3 year periodogram ordinate as the significantly larger long term period (i.e greater than 1 year period), along with 14.0 and 7.8 year periods. Fisher's κ test, also indicated the 23.3 year periodogram ordinate of the annual water levels statistically significant to the 1% level of significance, which is in agreement with the Grenander-Rosenblatt test.

Residual analysis of monthly average water levels showed variation about the mean with cyclic behavior, indicating a possible long term cyclicity of 70 to 80 year period. Although, there are not enough data for a full cycle, four quarter cycles of approximately 20 year periods can be distinguished in the residuals.

Table 2. **Periodogram Ordinate Test of Detrended Transformed Monthly Water Levels**

κ	% Probability	Period (Years)
83.90165	< 0.01	1.0000
59.14042	< 0.01	23.3333
20.70724	< 0.01	14.0000
18.89159	< 0.01	7.7778
13.48739	< 0.01	0.5000

Table 3. Periodogram Ordinate Test of Detrended and Transformed Annual Water Levels

κ	% Probability	Period (Years)
10.22386	0.03	23.3333
2.89373	24.40	7.7778
2.79433	7.40	14.0000
1.42174	98.18	4.3750
1.33718	96.77	4.6667

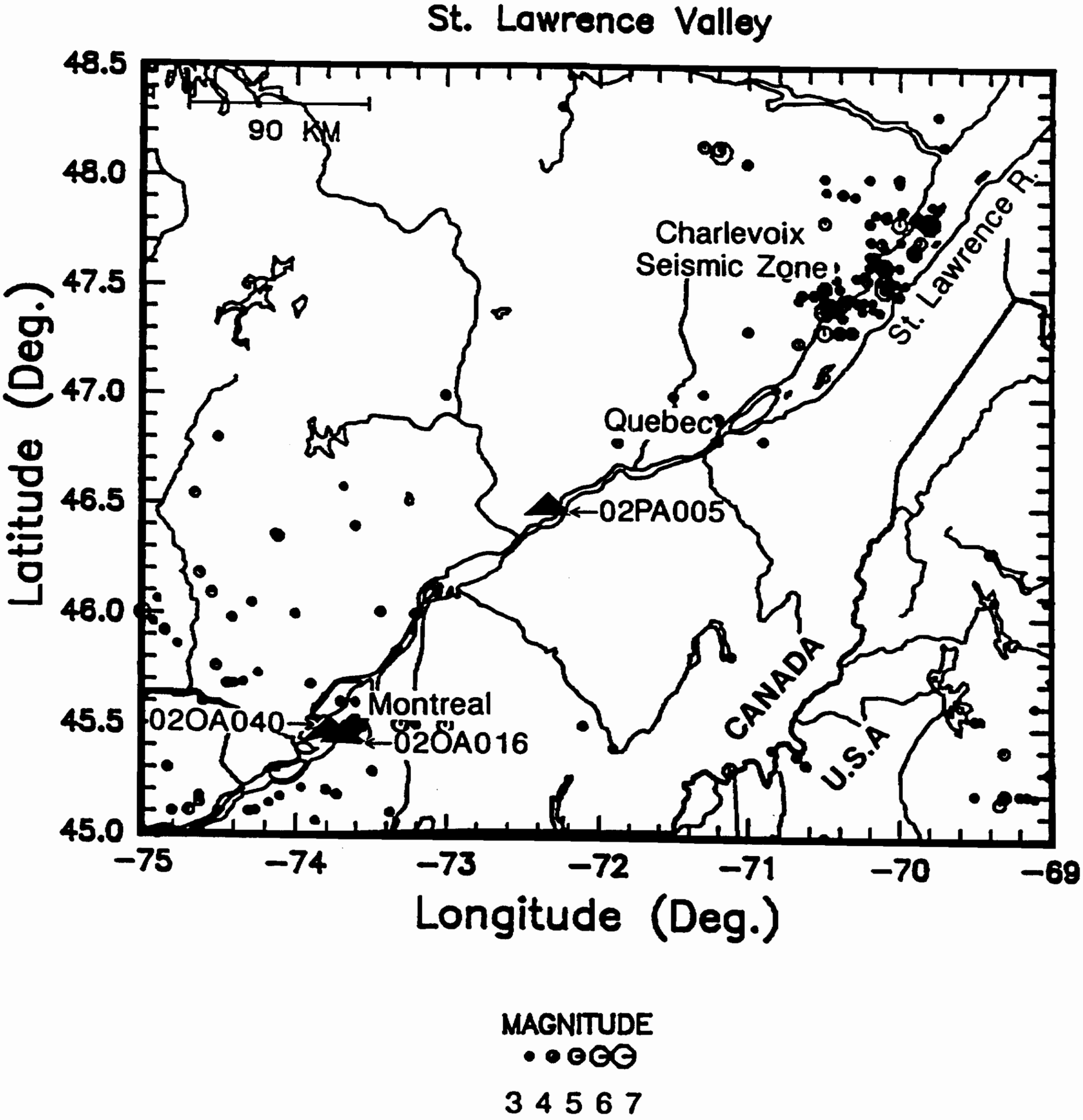

Figure 15. St. Lawrence Valley: Epicenter map of the St. Lawrence valley (M≥3.0), including the hydrometric stations, 02OA040 (water levels), 02OA016 (streamflow) and 02PA005 (water levels). Hydrometric station locations shown with closed triangles.

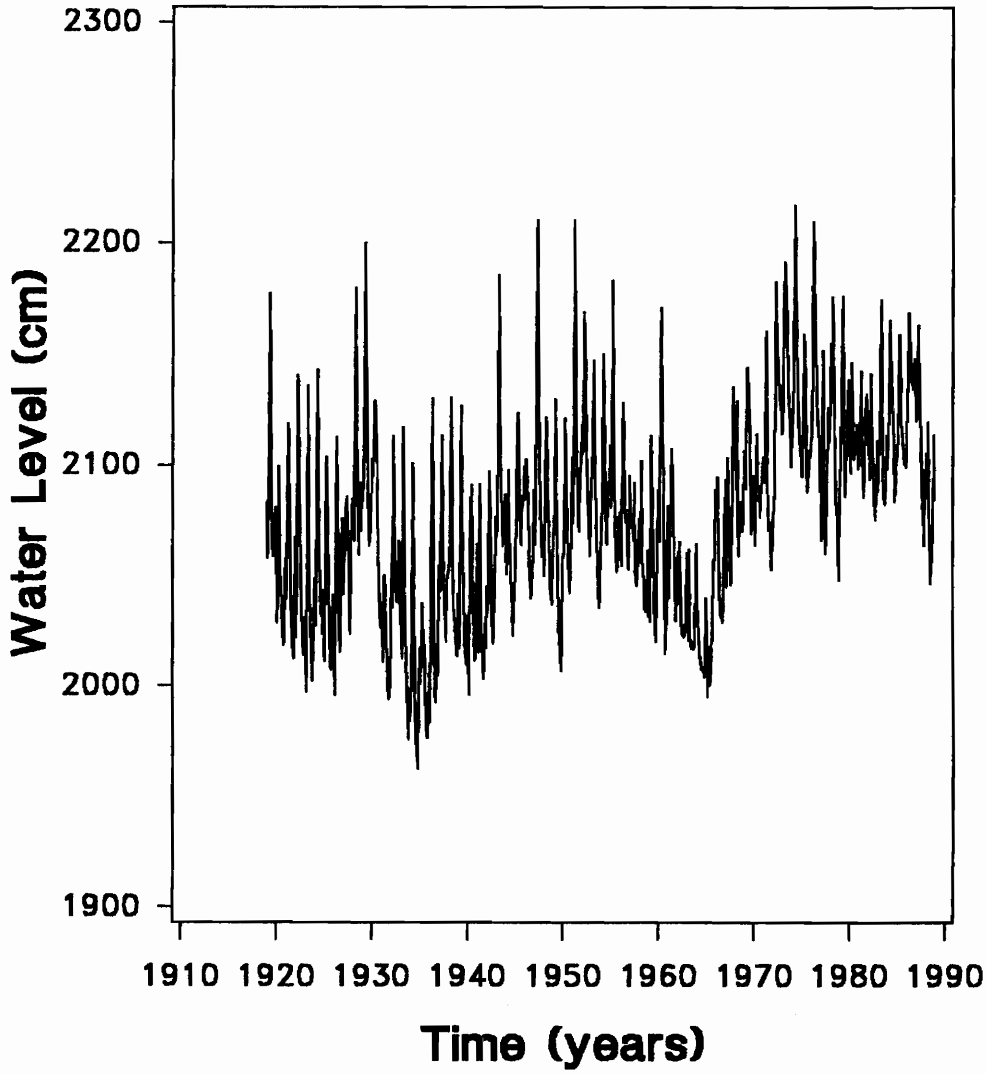

Figure 16. Monthly Water Levels: Average monthly water levels for the station 02OA040, for the 70 year period from 1919 to 1988.

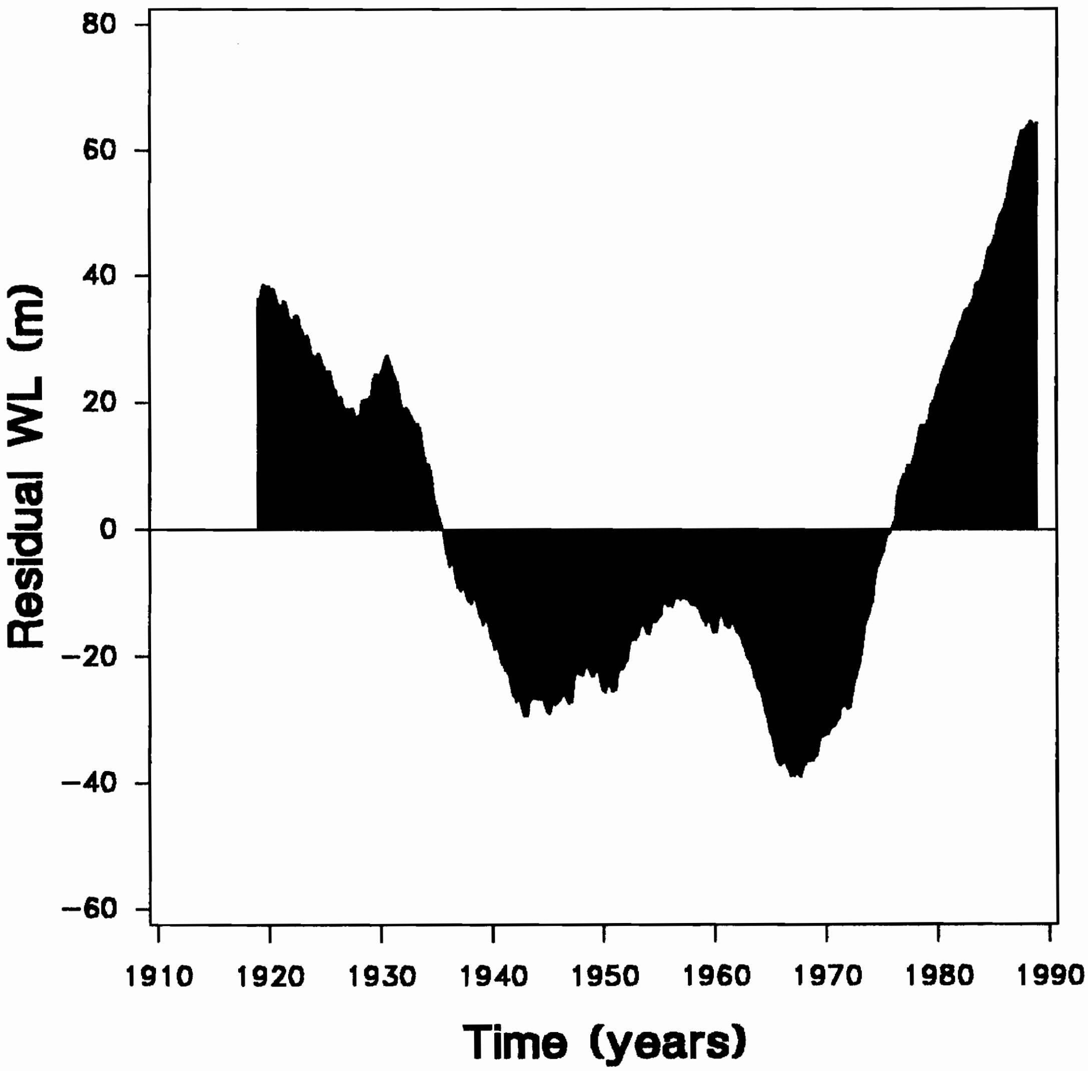

Figure 17. Residual Water Levels: Residual monthly water levels are obtained by subtracting the least squares fit from the cumulative water levels. Note the approximately 20 year long quarter cycles present in the residual time series.

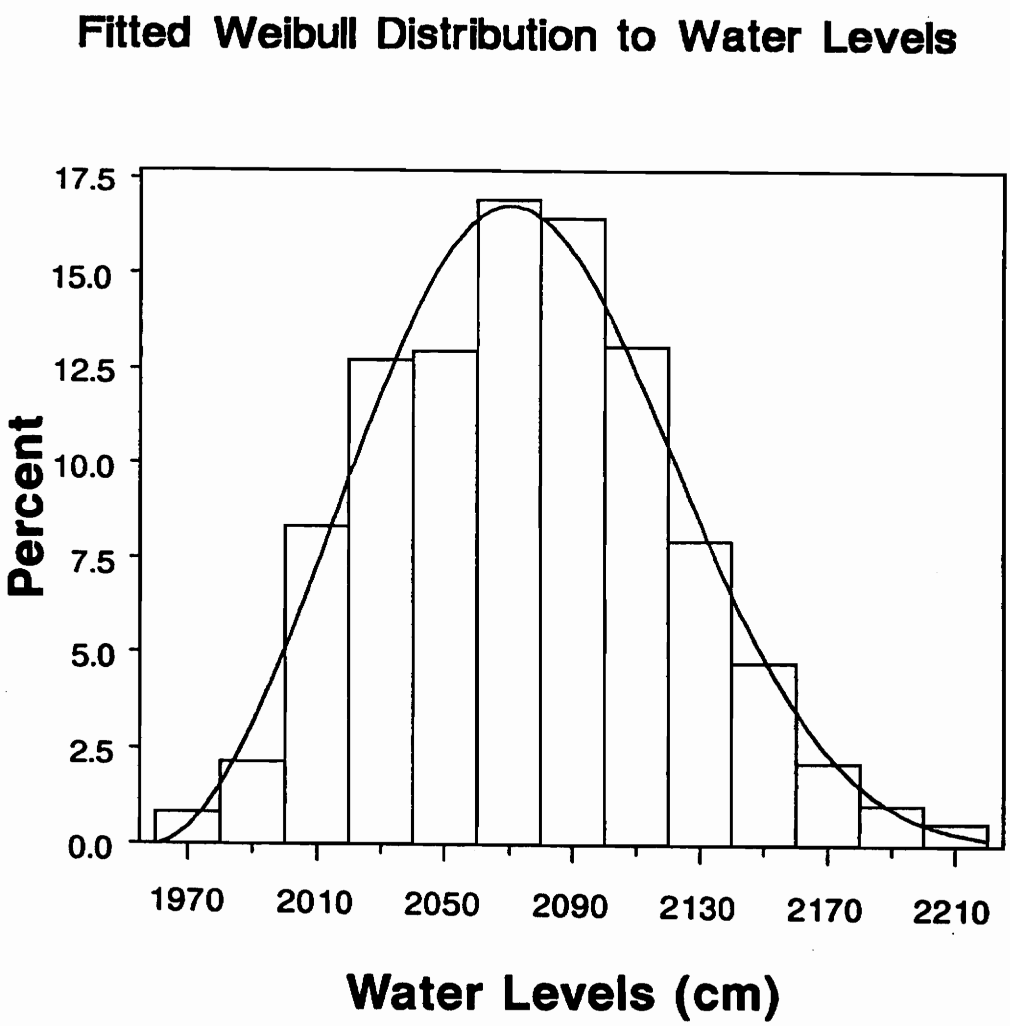

Figure 18. Monthly Water Levels Distribution: A Weibull distribution fitted to the monthly water level data with a resulting p-value=0.31 at the $\alpha=0.10$ (10%) level of significance. Because $p>\alpha$, the Weibull distribution is tested to fit the water level data.

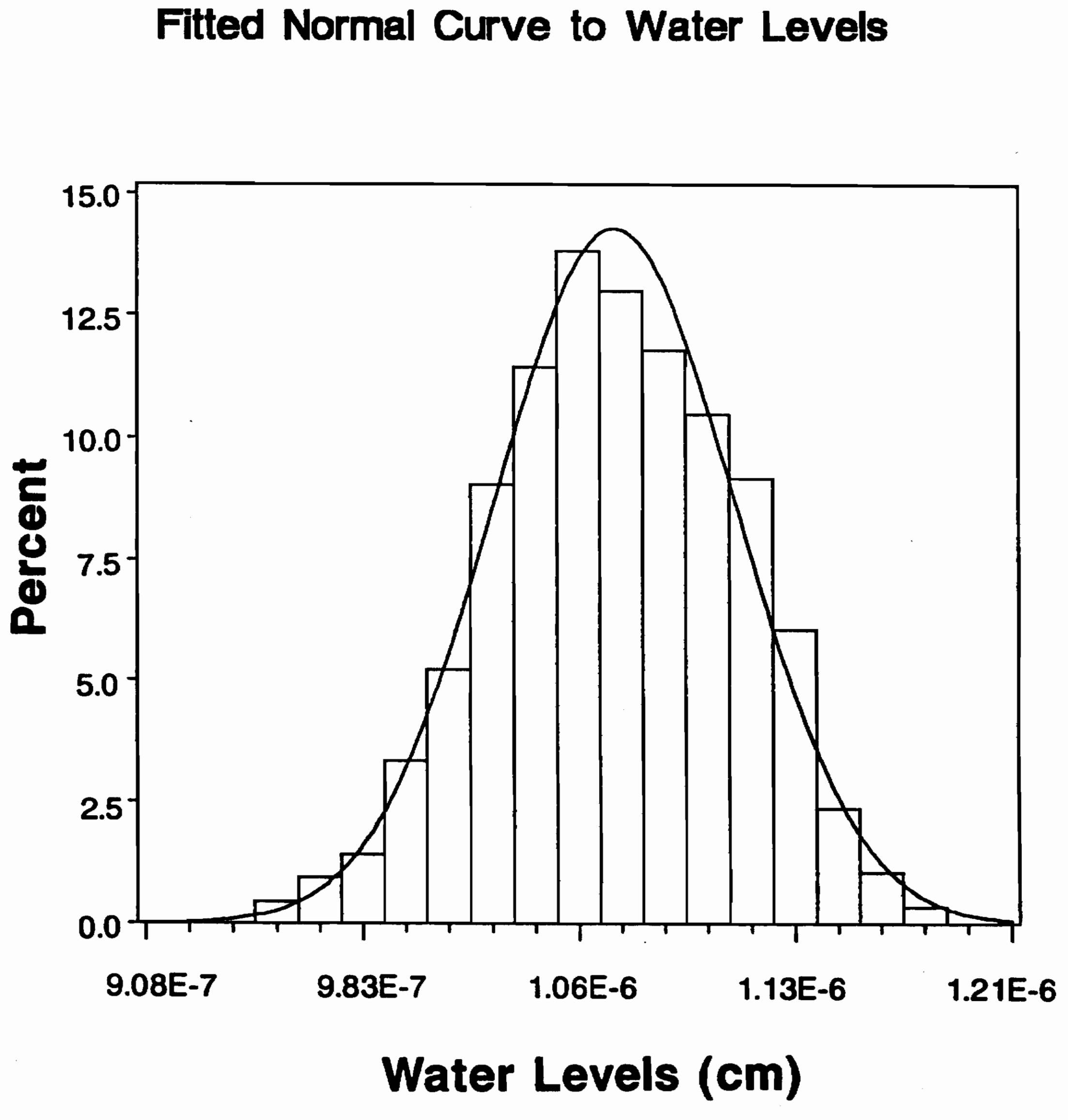

Figure 19. **Transformed Monthly Water Levels:** The monthly water levels are transformed to a normally distributed time series by $level = level^{\lambda}$, where $\lambda = -1.800$, is empirically determined; p-value $= 0.59 > 0.10 = \alpha$.

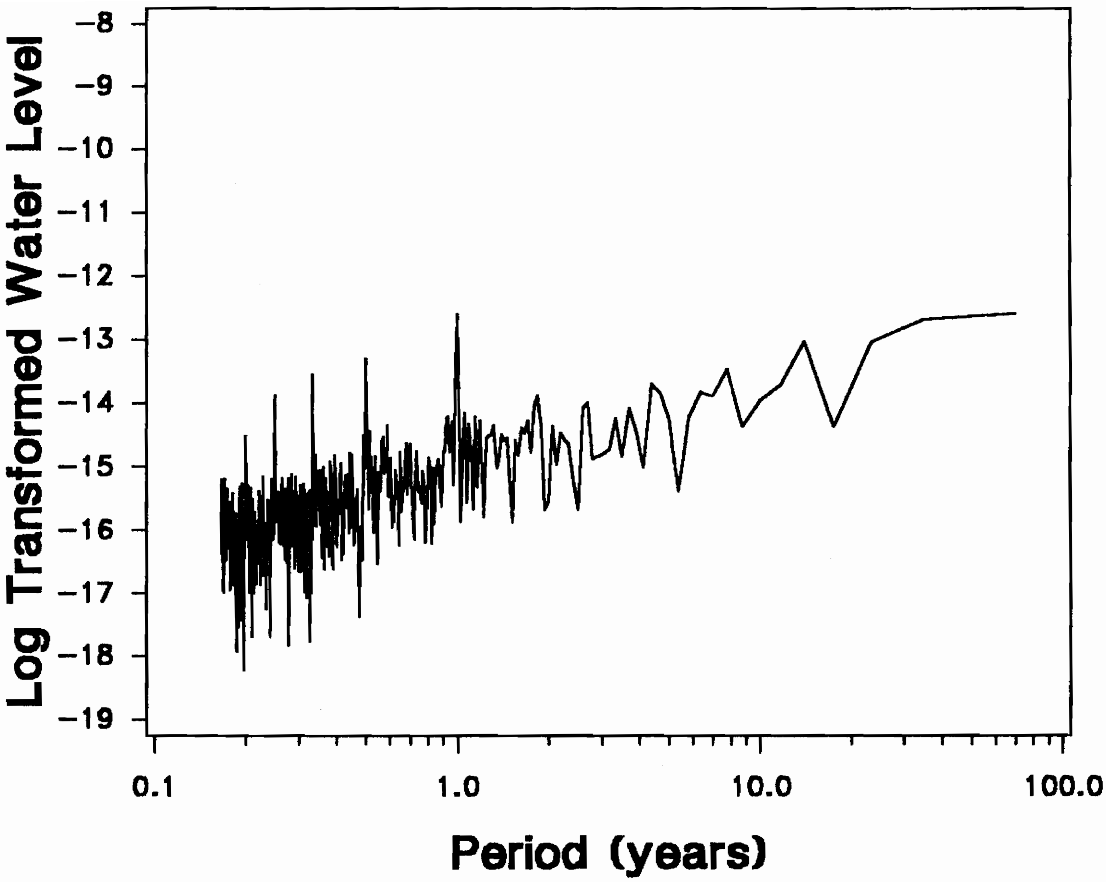

Figure 20. Periodogram of the Transformed Water Levels: Periodogram of the transformed to normally distributed monthly water levels for the station 02OA040. Note the largest periodogram ordinate at 1 year (the seasonal water cycle) and the second largest periodogram ordinate occurring at 70 years. Because of the 70 year length of the time series, the 70 year periodogram ordinate cannot be interpreted to correspond to a real periodic component in the time series.

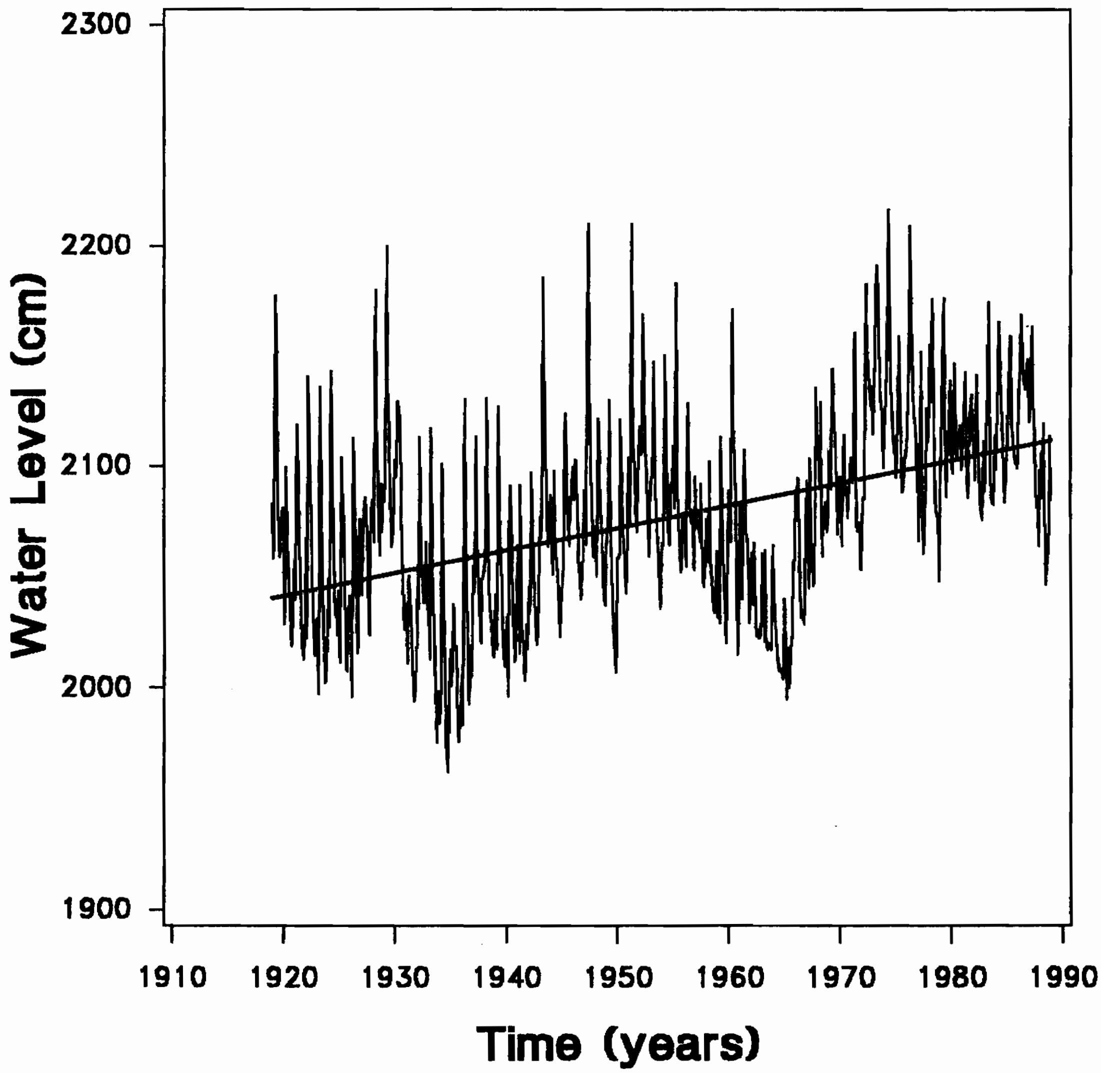

Figure 21. Straight Line Fit to the Water Levels: The 70 year long water level time series at station 02OA040 is fit with a straight line, by the least squares method. Note the trend (slope) of the line fit, indicating some long term variation in the water levels.

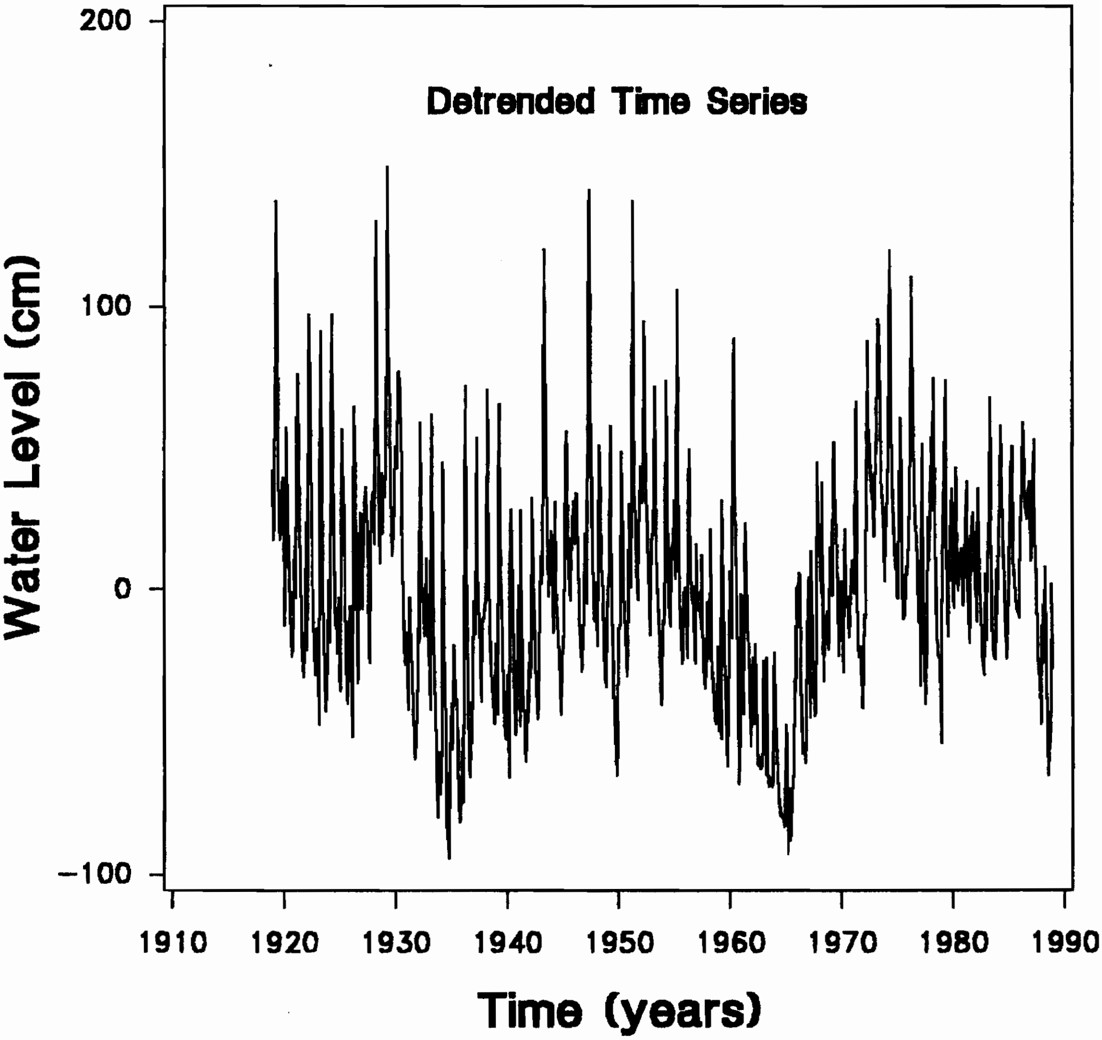

Figure 22. Detrended Water Level Time Series: The straight line fit is subtracted from the water levels resulting in the detrended water levels time series.

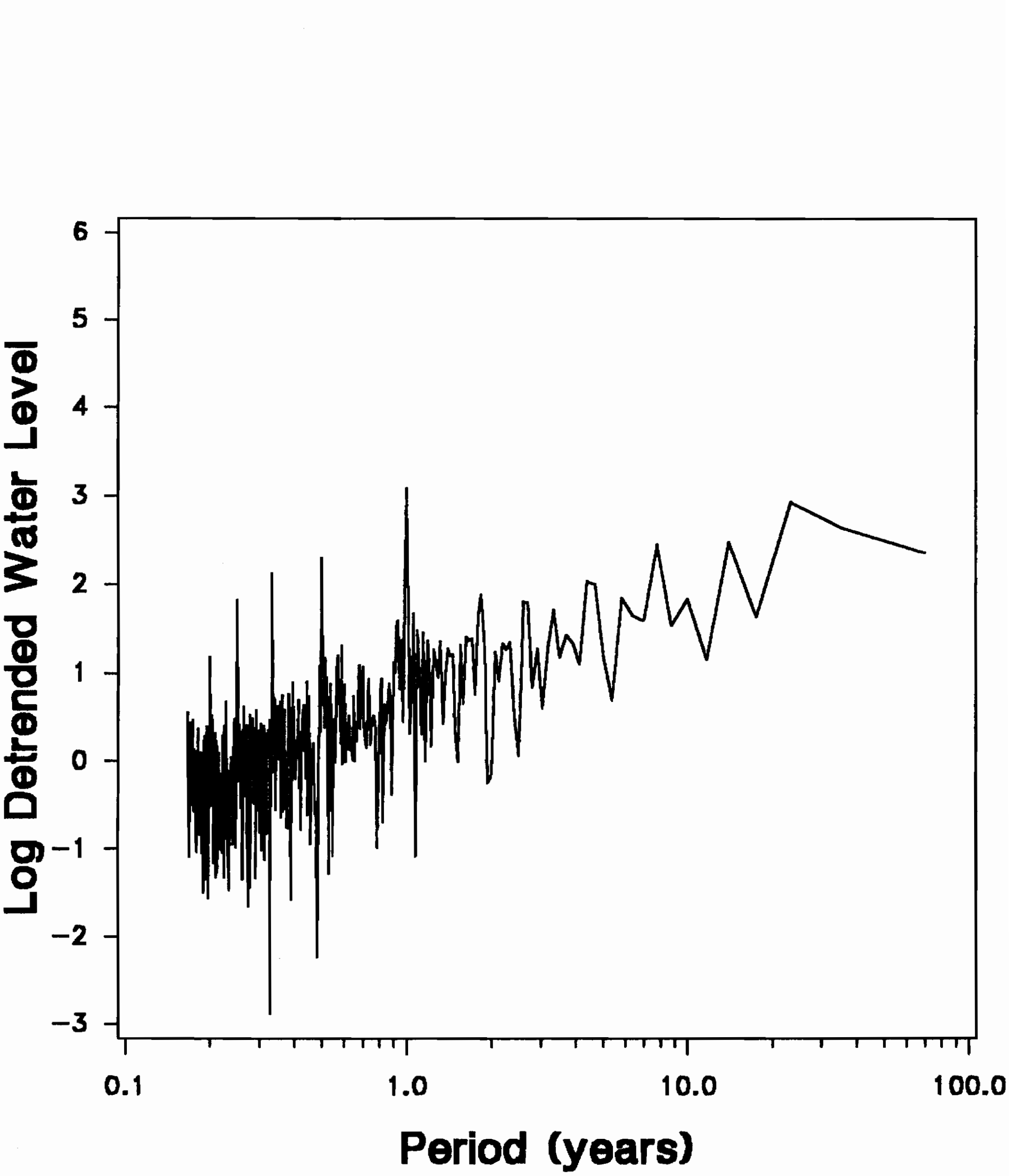

Figure 23. Periodogram of Detrended Water Levels: The periodogram of the detrended monthly water level time series yields the following periodogram ordinates in decreasing amplitude: 1.0, 23.3, 14.0 and 7.8 years.

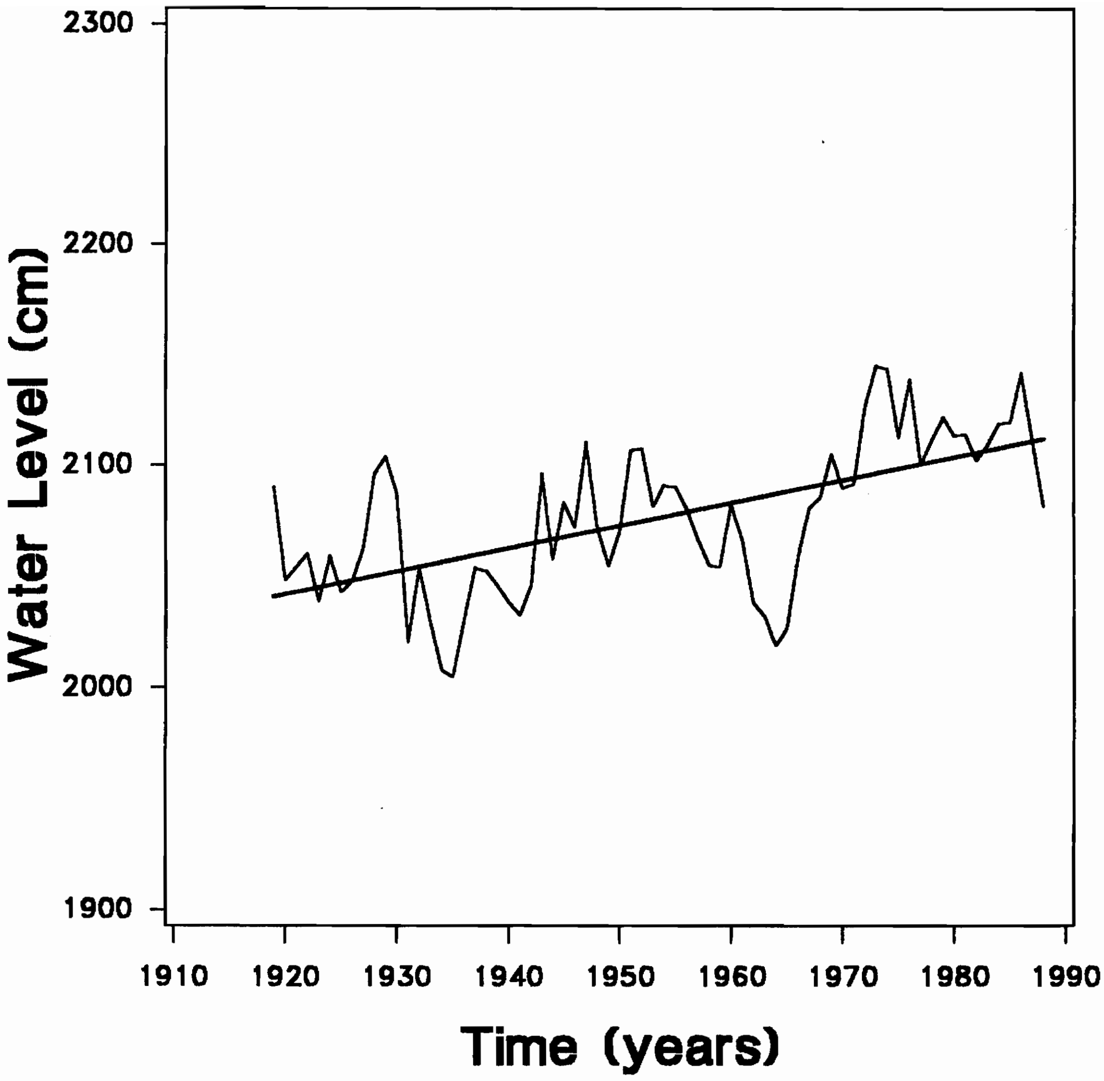

Figure 24. Annual Water Levels and Straight Line Fit: Average annual water levels for the station 02OA040, from 1919 to 1988, and a straight line fit by the least squares method.

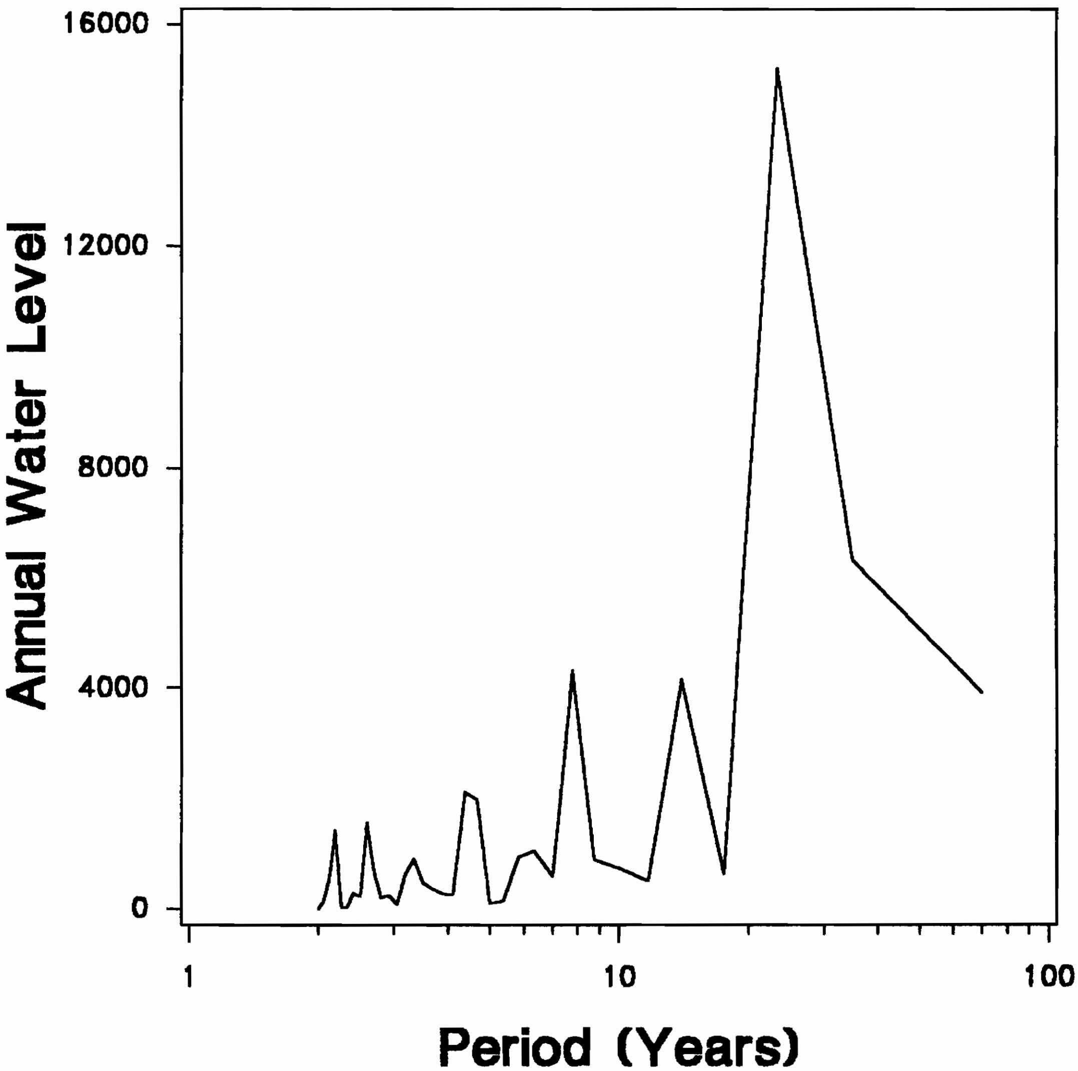

Figure 25. Periodogram of the Annual Water Levels: Periodogram of the detrended annual water levels for the station 02OA040, yields periodogram ordinates corresponding to periods of 23.3, 14.0 and 7.8 years.

Temporal Relationships Between Water Level and Seismicity

Group Delay Analysis

Possible time relationships between variations in the water level and in the strain factor time series are investigated using Group Delay analysis. The Group Delay $\tau(\omega)$ between two univariate time series represents the time lag between the time series as a function of a harmonic component at frequency ω (Foutz, 1980). The Group Delay analysis assumes that $\tau(\omega)$ varies with frequency. Tests were made for time relationships in a bandwidth of **m** frequencies, with center frequency of ω. Group Delay $\tau(\omega)$ is estimated by $p(\tau)$. Assuming the Fourier transform pairs of the water level [l(t), L(ω)] and seismicity [s(t), S(ω)] series,

$$p(\tau) = \frac{1}{m} \sum_{\omega=\omega_1}^{\omega_2} S(\omega)^{\bigstar} L(\omega) e^{+i\omega\tau}$$

where $\sum$ is the sum over the m frequencies, and $S(\omega)^{\star}$ is the complex conjugate of $S(\omega)$. A positive τ indicates that the harmonic component of center frequency ω of the second time series (water levels) leads the harmonic component of ω of the first time series (seismicity) by τ time units. Similarly, a negative τ would indicate that the harmonic of the first time series leads the harmonic of the second time series.

Group Delay analysis enables the investigation of time lag relationship between two time series over a bandwidth ω_1 to ω_2. That analysis was applied to the water level versus the seismic strain factor, and the water level versus the number of earthquakes. The harmonics selected for investigation correspond to principal periods of 23.3, 13.9, and 7.7 years. These three periods were statistically significant in the water level time series, and 13-14 year periods were statistically significant in the number of earthquakes time series, and present in the strain factor time series, as discussed in the previous sections. The time series analyzed consist of 70 years (1919 to 1988) of monthly water levels, monthly strain factor, and number of earthquakes per month with magnitudes $m_b \geq$ 5.0 (4 events) (see Figure 10) and $m_b \geq 4.5$ (7 events). For each pair of time series (water level vs strain factor; water level vs number of events), Group Delay analysis was applied to the center periods of 23.3, 13.9, and 7.7 years for bandwidths ranging from m = 9 to m = 81 period components.

The results of the analysis are summarized as follows. As expected, the two monthly number of events time series ($m_b \geq 5.0$ and $m_b \geq 4.5$) yielded the same time lag estimates and thus, their results will be referred as one set of results, from the number of earthquakes time series. The Group Delay analysis was found to be sensitive to the bandwidth selected. For $m < 20$, the time lag estimates varied widely at all center frequencies analyzed. For $m \geq 20$, the time lag estimates showed robust stability for the same center frequency at various values of m, for each of the pairs of time series analyzed. Group Delay analysis at the 23.3 year period failed to give consistent time lag estimates at all values of m, in both pairs of time series and, thus, it is excluded from the analysis. Either there is no time relationship between the two time series at the band of periods centered at 23.3 years, or the time series analyzed are not long enough.

The time lag estimates, p(τ), along with the corresponding Group Delay function amplitudes, for the center periods analyzed, 13.9 and 7.7 years, range from + 2.3 to + 4.1 years and are summarized in Table 4. The maximum value of the Group Delay function amplitude corresponds to the 13.9 year center period analysis and is shown in both water level versus number of earthquakes (Figure 26) and water level versus strain factor (Figure 27) Group Delay analyses. Note that the Group Delay function amplitudes corresponding to the 13.9 year center period are approximately twice as large as the Group Delay function amplitudes of the 7.7 year center period, as shown in. Table 4. Furthermore, the approximately 13 - 14 year harmonic tested statistically significant for the full length of 70 years of water levels and 200 years of seismicity, as stated in the preceding section. Therefore, the harmonic corresponding to a period of approximately 14 years is considered to be the dominant one in both water level and seismicity time series, with an associated time lag of + 2.3 years. It should be noted that, in Figure 27, the + 2.6 year time lag peak is slightly smaller than the -60.6 year time lag peak, and similarly in all the water level versus strain factor analyses, the negative longer time lag peak (approximately -60 years) is slightly larger than the shorter positive time lag peaks reported in Table 4. Because the -60.6 year Group Delay function peak has no physical meaning, i.e. the 14 year strain factor harmonic leading the 14 year water level harmonic by 60.6 years, the short positive time lags are believed to represent the best estimate of the time relationship between the time series, and, in particular, the + 2.3 year time lag determined from the water level vs. number of events analysis.

Positive time lags indicate that the water level harmonic components lead the seismicity harmonic components, allowing for a possible causal relationship between the two time series, as implied by the Hydroseismicity hypothesis. Negative time lags would indicate that the seismicity leads the water level harmonics.

The earth's crust is assumed to be a hydraulically diffusive fractured medium through which pore pressure transients are transmitted to hypocentral depths. Costain and Bollinger (1991) reviewed the one-dimensional model that describes the downward propagation of a plane pore pressure transient in a diffusive crust. The solution to the one dimensional diffusion equation for periodic fluctuations of surface hydraulic head indicates that the amplitude of the pore pressure transients at the surface are exponentially attenuated with depth, and that a frequency-dependent phase lag, linearly related to depth, is introduced. Furthermore, both pore pressure amplitude and phase lag depend on the period of the surface source (Costain and Bollinger, 1991). As illustrated by Major and Iverson (1988), longer periods of surface periodic variations are expected to penetrate deeper in the crust than shorter periods. The frequency dependence of the phase lag between surface pore pressure transients and pore pressure transients at depth, that are synchronous with seismicity variations according to the Hydroseismicity model, is shown in Table 4. Note that, if the 7.7 period is considered equally significant to the 14 year period, then, in opposition to what is expected (greater periods should correspond to larger time lags) the larger observed time lags correspond to shorter periods. The reversed order of the observed time lags, along with the considerably smaller 7.7 center period Group Delay function amplitude (compared to the corresponding 14 year center period) and the absence of a 7.7 periodicity in the seismicity time series, suggest that the time lag estimates for the 7.7 center period Group Delay analysis between the water levels and seismicity time series are not reliable.

Crustal diffusivity **D** values in the Charlevoix region are estimated using the relationship between phase velocity V_{ph} and Group Delay p(τ).

$$V_{ph} = 2\sqrt{\frac{D\pi}{T}} \quad \text{and} \quad V_{ph} = \frac{\textit{focal depth}}{p(\tau)}$$

The focal depth values of 7, 12 and 20 km used in the analysis correspond to the 10%, mean, and 90% quantile of depths, as determined from 631 network hypocenter locations (1974 - 1990) with ERZ $\leq$ 5.0 km (Figure 28), for magnitudes ranging from 0 to 5.0 (Figure 29) in the seismic zone. The crustal diffusivity estimates are shown in Table 5, and they correspond to the Group Delay estimates for the 14 year harmonic, from the water level versus number of earthquakes analysis. Those estimates appear more robust estimates of the time lag compared to the water level versus strain factor Group Delay analysis, and to the 7.7 year harmonic Group Delay analysis.

Thus, the Group Delay analysis implies crustal diffusivity values ranging one order of magnitude from 10.2 to 83.6 km^2/year (0.3 to 2.7 m^2/sec), which are within the range of published values (0.1 to 100 m^2/sec, or 3.2 to 3150 km^2/year), for the crust above the brittle-ductile transition (Li, 1985). The reverse order of crustal diffusivities in Table 5 from what would be expected, i.e. decreasing crustal diffusivity with increasing depth, is due to the fact that all diffusivity values (corresponding to different depths) were calculated for the same time lag estimate of +2.3 years. Although no direct correlation between depth and diffusivity can be made at the present, the range of diffusivities estimated is in good agreement with the actual ones. Comparable crustal diffusivity values were estimated by Setterquist (1989) for the Central Virginia region, ranging from 7.9 to 148 km^2/year for focal depths of 3 to 13 km.

Summary and Discussion of Group Delay Results

Spectral analysis of water levels and seismicity in the St. Lawrence valley indicates that there are periodicities present in both series of approximately 14 years. Group Delay analysis of harmonic components corresponding to periods ranging from 8 to 23 years of the water level versus number of earthquakes data sets, showed a maximum value of the Group Delay function for periods of 14 years (Figure 26). The corresponding time lag is +2.3 years, with the + sign indicating that the water level time series leads the seismicity time series. For the range of center periods studied, however, longer time lags correspond to shorter center periods and shorter time lags correspond to longer center periods of the Group Delay analysis (Table 4). The reverse order of time lag - center period relationship, along with the Group Delay function amplitudes and the statistical tests of the preceding sections, suggest that the 14 year period harmonic may be the dominant one in water level and seismicity time series. Therefore, conclusions of this study will be based primarily on the 14 year period harmonic.

Crustal diffusivity values estimated from the Group Delay analysis for the 14-year period are within one order of magnitude ranging from 10.2 km^2/year to 83.6 km^2/year. These values are within the expected range of values of diffusivity for the crust; however, no direct correlation between specific depths and diffusivities can be attempted at this stage.

The above results support the hypothesis of possible causal relationship between pore pressure changes at the surface (caused by water level changes) and seismicity (represented by the number of earthquakes and the strain factor). According to the Group Delay analysis, a pressure pulse associated with cyclic pore pressure changes of approximately 14 year period would require 2.3 years to diffuse to hypocentral depths. Attention should be drawn to the the physical process described by Hydroseismicity as a cyclical, but not periodic process, i.e. a repetitive process but not at constant time intervals. That is, a particular water level variation would not be associated with a particular seismic event 2.3 years later. However, as indicated by the results of the Group Delay analysis, the presence of cyclical harmonics in the surface pore pressure variations may trigger a similar cyclical behavior in the seismicity of the area.

Table 4. Group Delay Analysis Results

	Water Level vs S	Water Level vs N
Center Period (years)	**Time Lag** (years) **(Amplitude)**	**Time Lag** (years) **(Amplitude)**
7.7	+4.1 (2.5E9)	+4.0 (0.16)
13.9	+2.6 (4.3E9)	+2.3 (0.33)

Table 5. Crustal Diffusivity Estimates for the St. Lawrence Valley

	D $(\frac{km^2}{year})$
Focal Depth (km)	**Water Level Period** (years) 14
7	10.2
12	30.1
20	83.6

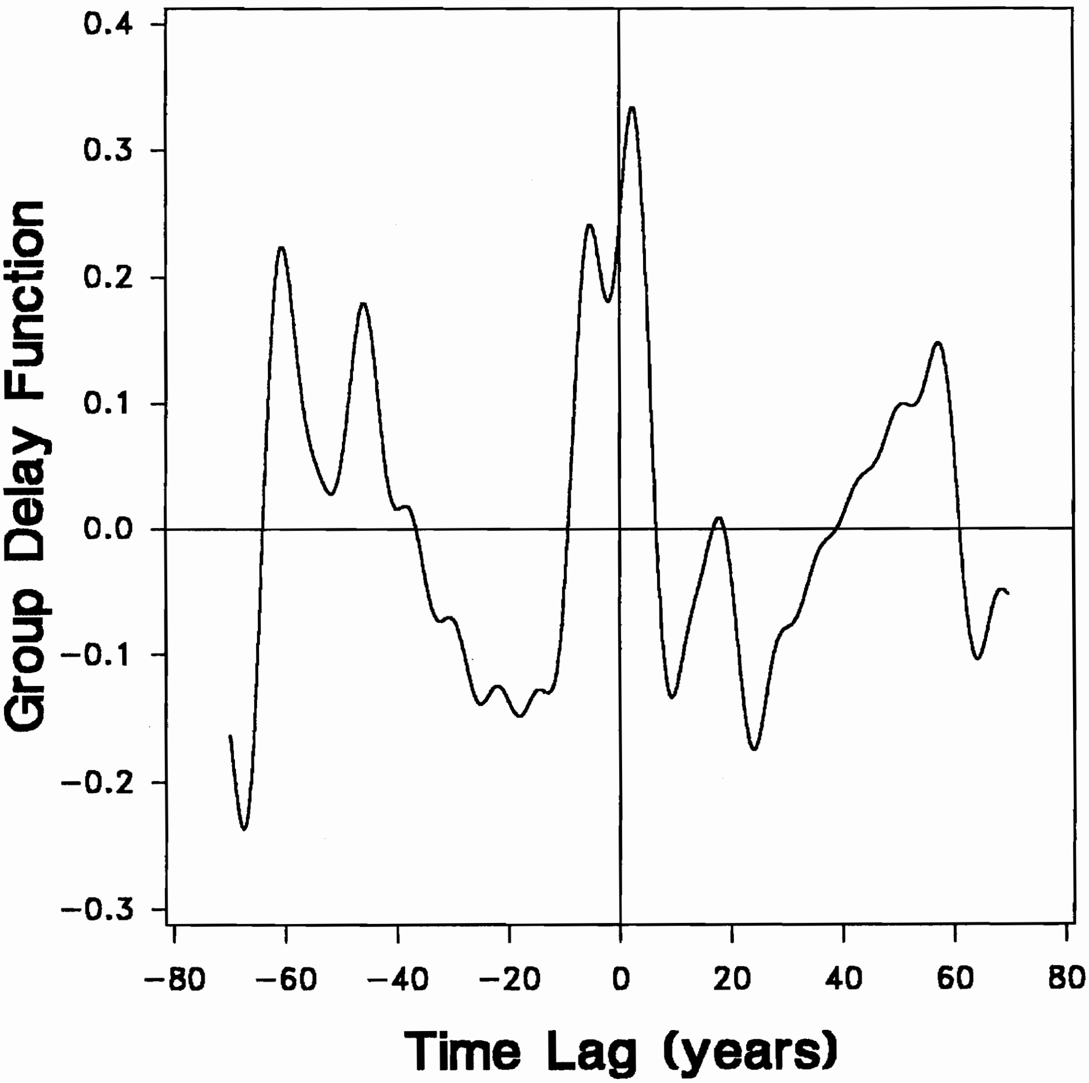

Figure 26. Group Delay p(τ) - Water Level and Number of Earthquakes: Group Delay of monthly water levels and monthly number of events ($m_b \geq 5.0$) data sets, at center period of 13.9 years, with bandwidth m=81, $\omega_1 = 7.8$, $\omega_2 = 69.9$ years. The Group Delay function shows a time lag of $\tau(\omega) = +2.3$ years, indicating that the water level time series leads the seismicity time series by 2.3 years.

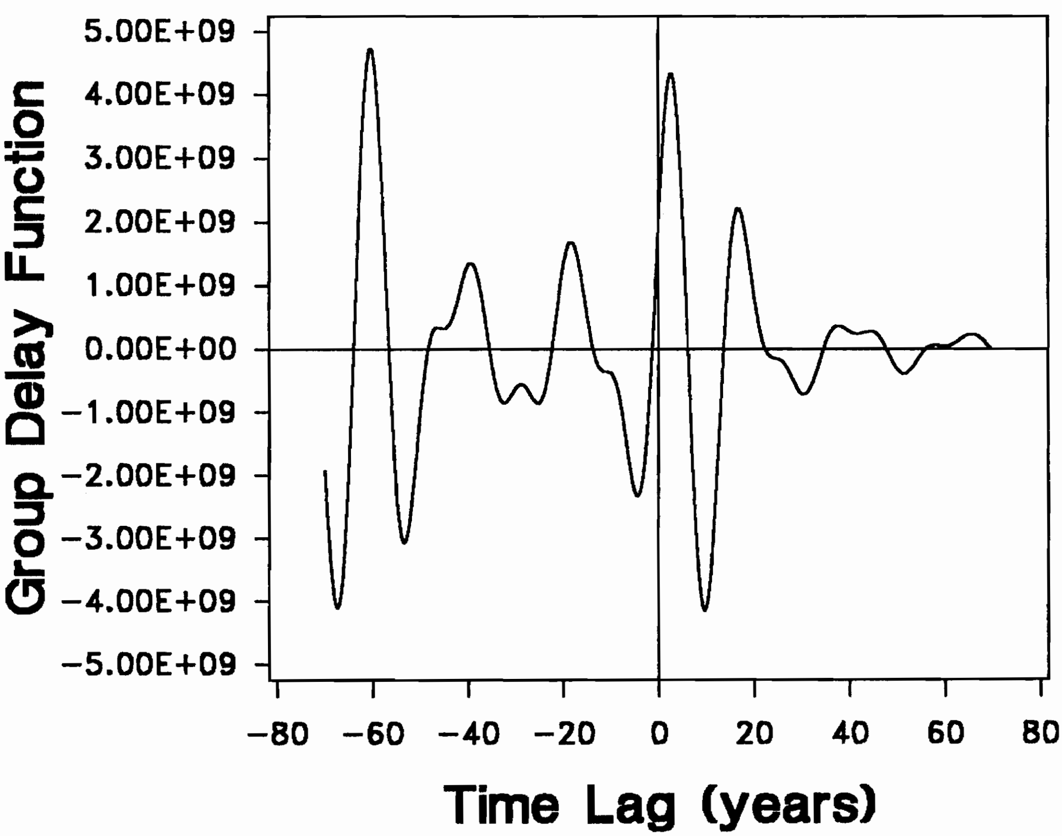

Figure 27. Group Delay p(τ) - Water Level and Strain Factor: Group Delay of monthly water levels and monthly strain factor data sets, at center period of 13.9 years, with bandwidth m = 41, $\omega_1 = 9.9$, $\omega_2 = 23.3$ years. The Group Delay function the largest amplitude at -60.6 years, and the second largest amplitude at + 2.6 years.

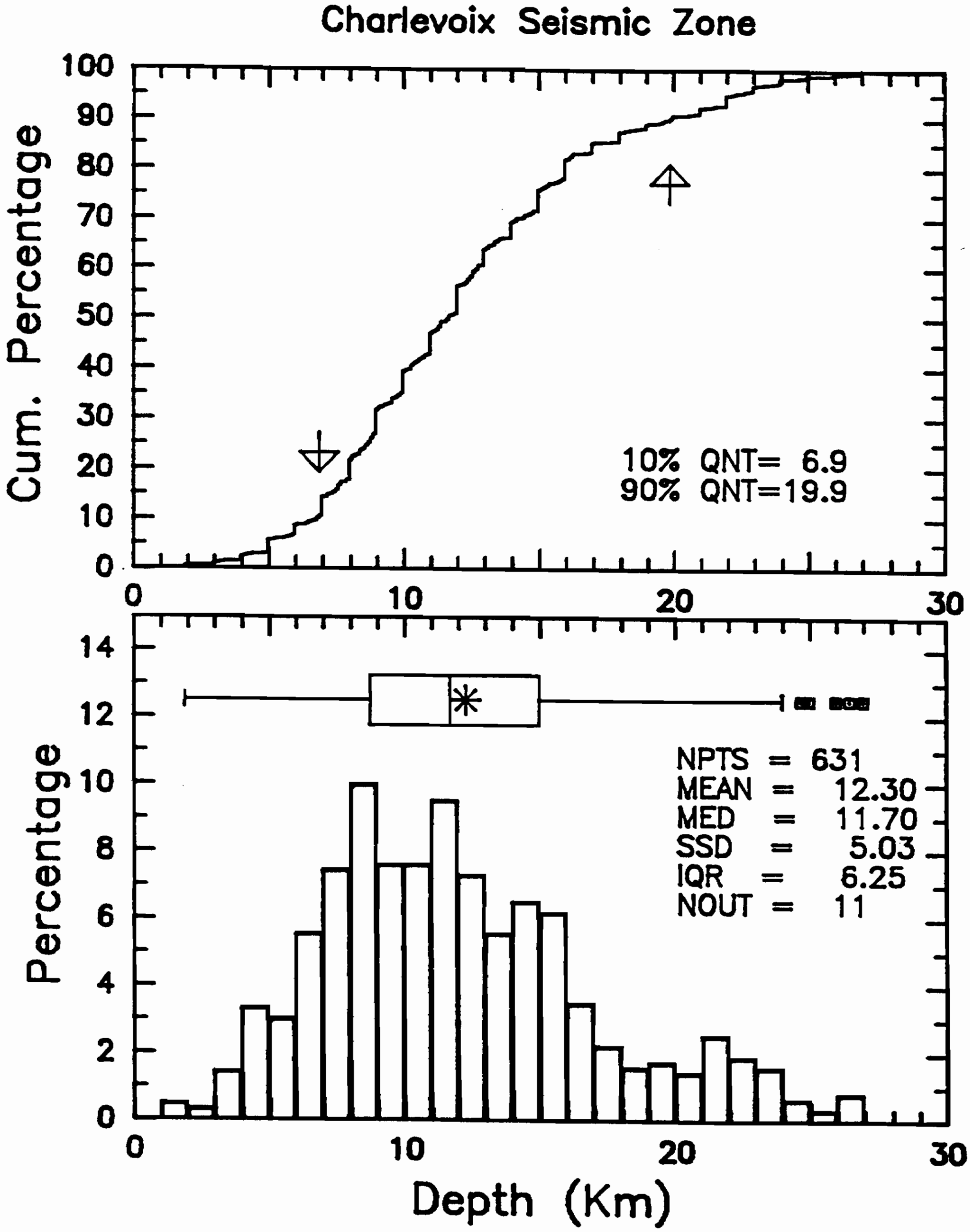

Figure 28. Earthquake Depth Distribution: Earthquake depth distribution in the Charlevoix Seismic Zone for 631 earthquakes (NPTS), from 1974 to 1990, with ERZ ≤ 5 km; pre-network depths prior to 1977 are unreliable. The MEAN depth for the seismic zone is 12.3 km, with a sample standard deviation 5.03 (SSD), interquartile range 6.25 (IQR), and 11 outliers (NOUT). The 10% quantile (QNT) depth is 6.9 km and the 90% quantile depth is 19.9 km. Source of data: The Canadian Earthquake Epicentre File, obtained from the Geological Survey of Canada.

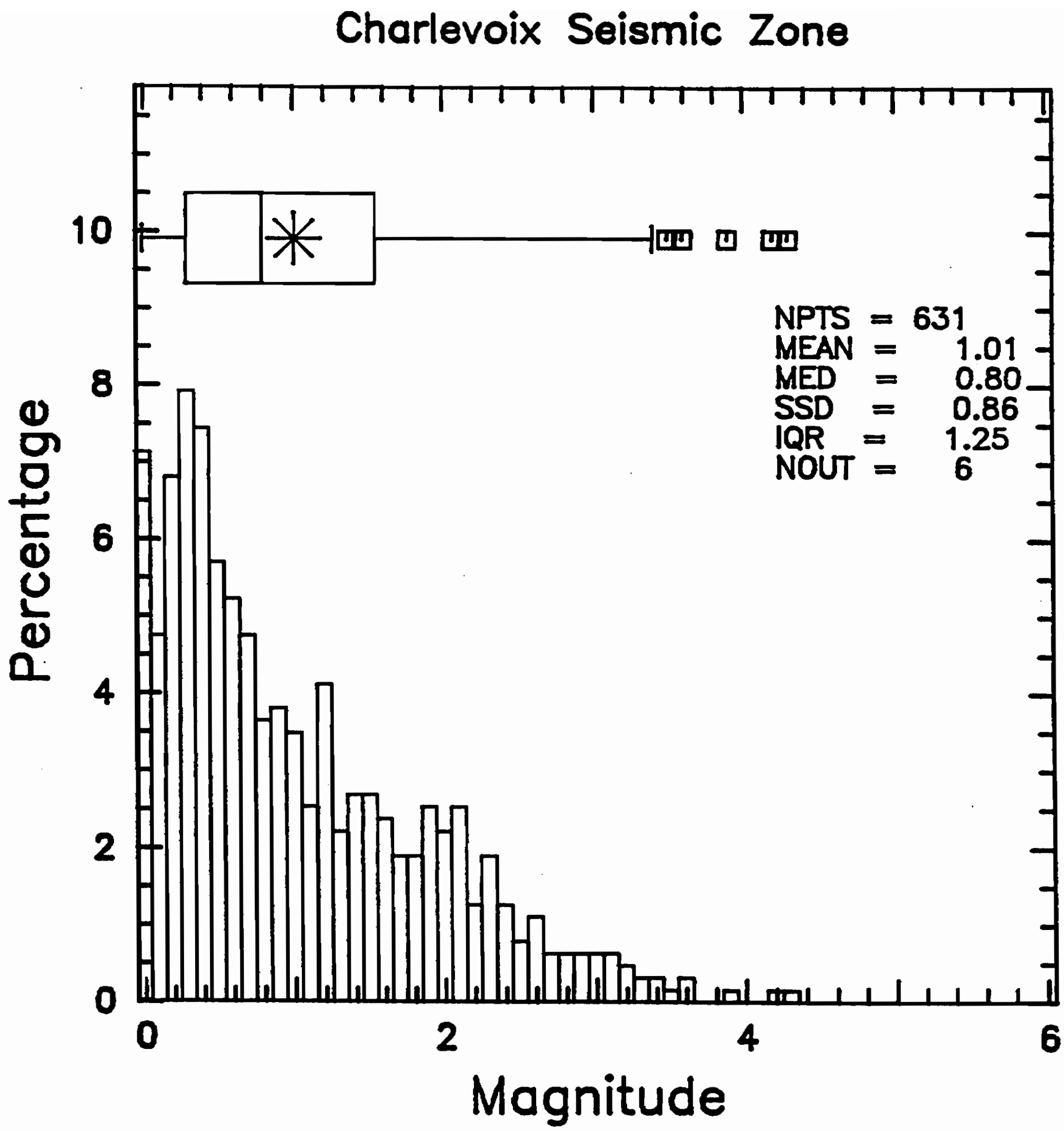

Figure 29. Magnitude Distribution: Earthquake magnitude distribution in the Charlevoix Seismic Zone for 631 earthquakes, from 1974 to 1990, with ERZ $\leq$ 5 km; The mean magnitude for the seismic zone is 1.01, with sample standard deviation 0.86, interquartile range 1.25, and 6 outliers. Source of data: The Canadian Earthquake Epicentre File, obtained from the Geological Survey of Canada.

Summary and Conclusions

Analyses of water levels and seismicity in the Charlevoix region along with the supported conclusions are summarized in the following.

- To characterize the temporal release of seismic energy in the Charlevoix seismic zone, two measures of the seismic activity are considered in the 200 year record of seismicity: the strain factor (magnitude dependent) and the number of earthquakes per unit time (magnitude independent).

- Residual analysis of the annual strain factor indicates cyclical, but not periodic, variation about the mean value of seismic activity, with long term cycles of approximately 65 to 70 years.

- Fourier spectral analyses of the strain factor and of the number of earthquakes data sets indicate common short term cyclicities at 13 to 14 year periods and long term cyclicities at 55 to 70 years. Similar analyses at varying lengths of strain factor data sets (200, 140 and 90 years long) and varying threshold magnitudes of number of earthquakes data sets (m_b of 4.5, 5.0 and 5.5) yield the same temporal characteristics (13.4 and 67 year cycles) suggesting stability of the analysis procedure.

- Fisher's periodogram ordinate test is applied to the spectral analyses results to determine the significance of the largest periodogram ordinate, observed at 13.4 years, with respect to the average. The number of earthquakes per year analysis yielded a statistically significant periodogram ordinate at 13.4 years at the 10% level of significance, whereas the annual strain factor analysis failed to test statistically significant the 13.4 year ordinate. The sensitivity of the spectral analysis and Fisher's statistical test to the binning of the time series, and, consequently, to the number of periodogram ordinates, is tested applying the same analysis to the *monthly* strain factor and to the number of earthquakes *every two years*. Similar spectral and statistical results were obtained thereby indicating stability in the analysis procedure and the cyclicity results. Although the strain factor 13.4 year periodogram ordinate did not test statistically significant, it is in agreement with the statistically significant number of earthquakes 13.4 year periodogram ordinate.

- Seventy years of monthly water level fluctuations in the St. Lawrence river are analyzed to characterize the temporal behavior of the water table fluctuations in the St. Lawrence valley. In this study, water table fluctuations are considered the source of pore pressure pulses diffused in the crust.

- Residual analysis of the monthly water levels indicate a cyclical process, with a long term cycle of approximately 70 to possibly 80 years. Although one complete full cycle is not present in the available data, 4 quarter cycles can be distinguished in the residuals.

- Fourier spectral analysis of the water level data set indicates the seasonal water cycle peak at 1 year as the largest periodogram ordinate, as expected, and shows peaks at longer periods of 23, 14 and 8 years. Because of the short length of the time series (70 years) periodogram ordinates corresponding to periodicities greater than 35 years cannot be interpreted to correspond to real periodic components in the time series.

- The Grenander-Rosenblatt method tests for the statistical significance of more than one periodogram ordinates, under the hypothesis that the time series is normally distributed (Priestley, 1981). Therefore, the Weibull distributed water level time series is transformed to a normal distribution using the Box-Cox power transformation (Box and Cox, 1964). The Grenander-Rosenblatt method applied to the transformed data indicated that the 1, 23, 14, and 8 year periodogram ordinates were significant with respect to the remaining periodogram ordinates. Application of the same analysis on the *annual* water levels yields similar results, thereby indicating stability of the results for two different data binnings.

- The water level and seismicity data sets in the Charlevoix region both exhibit cyclical temporal behavior, with common cyclicities of approximately 14 years. These common cyclicities are investigated for temporal (time lag) relationships using Group Delay analysis, which is applied to two pairs of data (water level and number of earthquakes; water level and strain factor), for center periods of 8 to 23 years. The maximum value of the Group Delay function occurs at 14 years with a corresponding time lag of +2.3 years, with the water levels **leading** the seismicity time series.

- From the results of the Group Delay analysis, longer time lags correspond to shorter center periods and shorter time lags correspond to longer center periods. This relationship is the reverse from what expected, if periods other than 14 years are indeed statistically significant. However, in this analysis the 14 year period harmonic is considered the dominant one in water level and seismicity time series.

- Crustal diffusivity values estimated from the Group Delay analysis for a center period of 13 to 14 years, range between 0.3 m^2/sec and 2.7 m^2/sec for a range of depths of 7 to 20 km. These values are within the expected range of 0.1 to 100 m^2/sec (Li, 1985). Direct correlation between depth and crustal diffusivity is not justified with the available data base and results.

- The results from this study suggest a possible causal relationship between the repetitive mechanical effects of pore pressure transients and seismicity in the Charlevoix seismic zone. Except for the uncertain reversed order relationship between the period of pore pressure variation and time lag in seismic activity, the temporal behavior of the physical processes studied in the Charlevoix region, are in agreement with the Hydroseismicity model proposed by Costain and co-workers.

Bibliography

Ang, A. and Tang, W.H., 1975. Probability concepts in Engineering planning and design, volume 1, basic principles. John Wiley & Sons, N.Y., 114-123.

Anglin, F.M., 1984. Seismicity and faulting in the Charlevoix zone of the St. Lawrence Valley. Bull. Seism. Soc. Am., 74: 595-603.

Box, G.E.P. and Cox, D.R., 1964. An analysis of transformations. J. Royal Statistics Soc., B-26: 211-252.

Buchbinder, G.G.R., Lambert, A., Kurtz, R.D., Bower, D.R., Anglin, F.M. and Peters, J., 1988. Twelve years of geophysical research in the Charlevoix seismic zone. Tectonophysics, 156: 193-224.

Cornell, C.A. and Winterstein, S.R., 1988. Temporal and magnitude dependence in earthquake recurrence models. Bull. Seism. Soc. Am., 78: 1522-1537.

Costain, J.K., Bollinger, G.A. and Speer, J.A., 1987a. Hydroseismicity: a hypothesis for the role of water in the generation of intraplate seismicity. Seismol. Res. Lett., 58: 41-64.

Costain, J.K., Bollinger, G.A. and Speer, J.A., 1987b. Hydroseismicity: a hypothesis for the role of water in the generation of intraplate seismicity. Geology, 15: 618-621.

Costain, J.K., Bollinger, G.A. and Speer, J.A., 1988. Reply to comment from J.J. Major and R.M. Iverson on "Hydroseismicity-A hypothesis for the role of water in the generation of intraplate seismicity". Geology, 16: 563-564.

Costain, J.K. and Bollinger, G.A., 1991. Correlations between streamflow and intraplate seismicity in the central Virginia, U.S.A., seismic zone: evidence of possible climatic controls. Tectonophysics, 186: 193-214.

Doig, R., 1990. 2300 yr history of seismicity from silting events in Lake Tadoussac, Charlevoix, Quebec. Geology, 18: 820-823.

Environment of Canada, 1989. Quebec historical streamflow summary. Cat. No. En 36-418/1988-8.

Evans, D.M., 1966. The Denver area earthquakes and the Rocky Mountain Arsenal disposal well. Mountain Geol., 3: 23-36.

Fisher, R.A., 1929. Tests of significance in harmonic analysis. Proceedings of the Royal Society in London, series A, 125: 54-59.

Foutz, R.V., 1980. Estimation of a common group delay between two multiple time series. J. Am. Stat. Assoc., 74: 779-788.

Freeze, R.A. and Cherry, J.A., 1979. Groundwater. Prentice Hall, Englewood Cliffs, N.J., 604 pp.

Fuller, W., 1976. Introduction to statistical time series, John Wiley and Sons.

Gardner, J.K. and Knopoff, L., 1974. Is the sequence of earthquakes in southern California, with aftershocks removed, Poissonian? Bull. Seism. Soc. Am., 64: 1363-1367.

Hasegawa, H.S. and Wetmiller, R.J., 1980. The Charlevoix earthquake of 19 August 1979 and its seismo-tectonic environment. Earthquake Notes, 51: 23-37.

Hasegawa, H.S., 1986. Seismotectonics in eastern Canada: An overview with emphasis on the Charlevoix and Miramichi regions. Earthquake Notes, 57: 83-94.

Huang, J. and Turcotte, D.L., 1990. Are earthquakes an example of deterministic chaos? Geophys. Res. Lett., 17: 223-226.

Ito, K. and Matsuzaki, M., 1990. Earthquakes as self organized critical phenomena. J. Geophys. Res., 95: 6853-6860.

Lamontagne, M., 1987. Seismic activity and structural features in the Charlevoix region. Can. J. Earth Sci., 24: 2118-2129.

Leblanc, G. and Buchbinder, G., 1977. Second microearthquake survey of the St. Lawrence Valley near La Malbaie, Quebec. Can. J. Earth Sci., 14: 2778-2789.

Leblanc, G. and Anglin, F.M., 1978. Induced seismicity at the Manic 3 reservoir, Quebec. Bull. Seism. Soc. Am., 68: 1469-1485. Can. J. Earth Sci., 14: 2778-2789.

Li, V.C., 1985. Estimation of in-situ hydraulic diffusivity of rock masses, J. Pure and Applied Geophys., 122: 545-559.

Lewis, P.A.W., 1970. Remarks on theory , computation and application of the spectral analysis of series of events. J. Sound Vib., 12: 353-375.

Mento, D.J., Ervin, C.P. and McGinnis, L.D., 1986. Periodic energy release in the New Madrid seismic zone. Bull. Seism. Soc. Am., 76: 1001-1009.

Nava, S.J., 1983. The New Madrid Seismic Zone: a test case for naturally induced seismicity. M. S. Degree in Geology, Memphis State Univ., Memphis, Tenn., 128 pp.

Nava, S.J. and Johnston, A.C., 1984. Rivers and earthquakes: a correlation for New Madrid and Mississippi River. Earthquake Notes, 55: 15.

Priestley, M.B., 1981. Spectral analysis and time series. Academic Press, N.Y., 890 pp.

Rondot, J., 1968. Nouvel impact météoritique fossil. La structure semi-circulaire de Charlevoix. Can. J. Earth Sci., 5: 1305-1317.

Rondot, J., 1970. La structure du Charlevoix comparée à d'autre impacts météoritiques. Can. J. Earth Sci., 7: 1194-1202.

Rondot, J., 1971. Impacite of the Charlevoix structure, Quebec, Canada. J. Geoph. Res., 76: 5414-5423.

Rondot, J., 1972a. La transgression ordovicienne dans le compté de Charlevoix, Québec. Can. J. Earth Sci., 9: 1187-1203.

SAS Institute Inc. SAS/ETS User's Guide, Version 5 Edition. Cary, N.C.: SAS institute Inc., 1984.738 pp.

SAS Institute Inc. SAS/QC Software, Version 6 Edition. Cary, N.C.: SAS institute Inc., 1989.660 pp.

Setterquist, S. and Sibol, M., 1988. Energy release cyclicity in the central Virginia seismic zone. Seismol. Res. Lett., 58: 104.

Setterquist, S., 1989. Temporal and spatial correlations between seismicity and streamflow volume in the central Virginia seismic zone. M.S. Degree in Geophysics, Virginia Polytechnic Institute and State University, Blacksburg, Va, 89 pp.

Sibol, M.S., Bollinger, G.A. and Birch, J.B., 1987. Estimation of magnitudes in central and eastern North America using intensity and felt area. Bull. Seism. Soc. Am., 77: 1635-1654.

Simpson, D.W., 1976. Seismicity changes associated with reservoir loading. Engineering Geology, 10: 123-150.

Simpson, D.W. and Negmatullaev, S.K., 1981. Induced seismicity at Nurek reservoir, Tadjikistan, USSR. Bull. Seism. Soc. Am., 71: 1561-1586.

Simpson, D.W., 1987. Triggered Earthquakes. Lamont-Doherty Geological Observatory of Columbia University, 1983-1986: 43-50.

Solomon, S.C. and Duxbury, E.D., 1987. A test of the longevity of impact-induced faults as preferred sites for later tectonic activity. J. Geoph. Res., Supplement, Proceedings of the 17th Lunar and Planetary Science Conference, 92: (B4), 759-768.

Talebi, S. and Cornet, F., 1987. Analysis of the microseismicity induced by a fluid injection in a granitic rock mass. Geophys. Res. Lett., 14: 227-230.

Talwani, P. and Acree, S., 1985. Pore pressure diffusion and the mechanism of reservoir-induced seismicity. J. Pure Appl. Geophys., 122: 947-965.

Appendix A. Temporal Relationship Between Water Levels at Stations 02OA040 and 02PA005

The temporal relationship between water levels at hydrometric stations 02OA040 and 02PA005 is determined to allow inferences on the water level fluctuations in the St. Lawrence valley. For the 14 common years of monthly average water level observations (1964-1977), each data set is normalized, i.e. the mean water level value for the entire time series is subtracted from each observation, and plotted in Figure 30 (source of data: Water Survey of Canada). Note the agreement between peaks and troughs in the two time series, except for the four month period, 12/67 to 3/68, where data are missing for the station 02PA005.

Regression analysis is applied to the monthly water level data sets. The analysis yielded that a linear relationship is a very good approximation, with sample correlation coefficient $r = 0.9$ for the model $[02PA005] = b_0 + b_1[02OA040]$. The two water level data sets correlate very well, despite the 180 km spatial separation of the hydrometric stations. Therefore, water levels at station 02OA040 can be assumed to represent water level fluctuations in the St. Lawrence river.

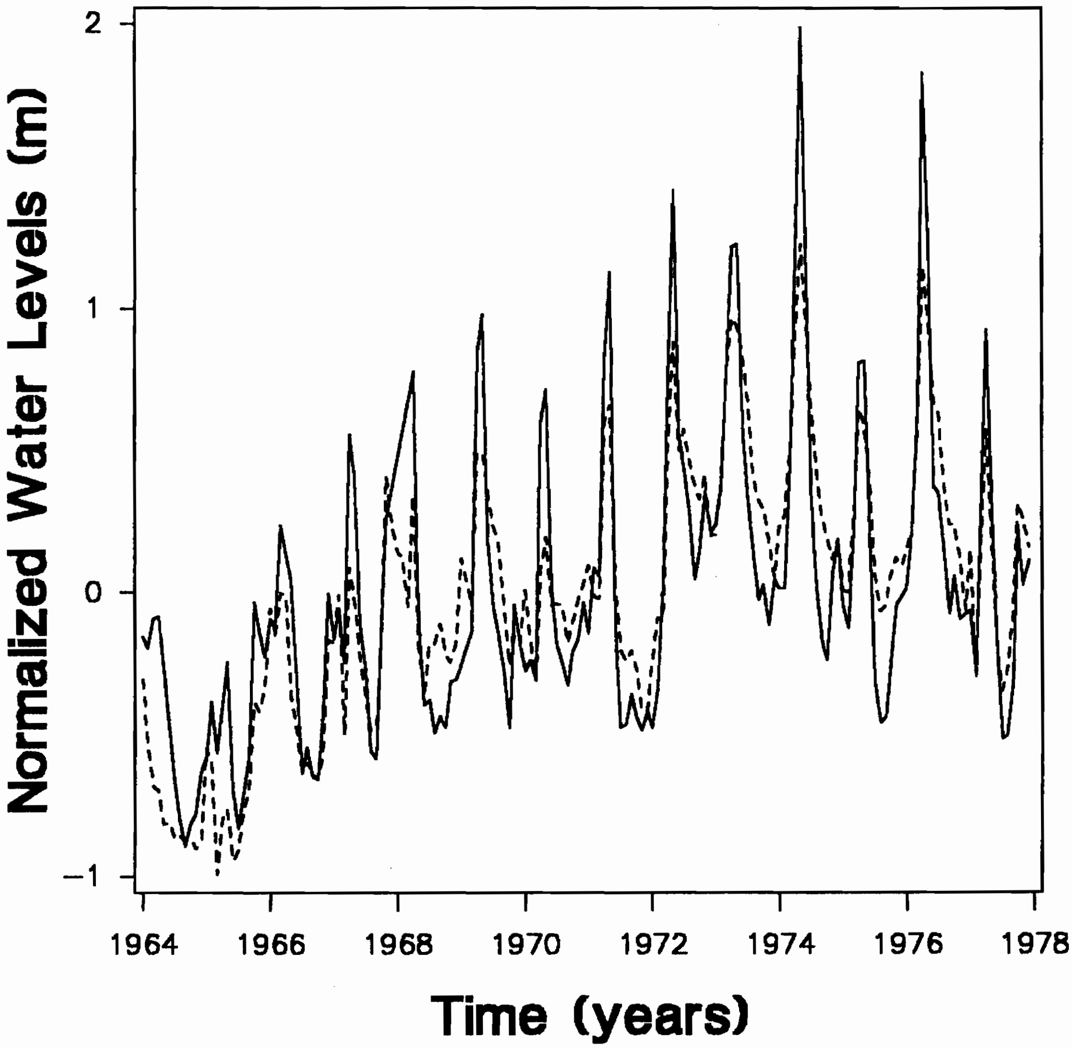

Figure 30. Normalized Water Levels at Stations 02OA040 and 02PA005: Normalized average monthly water levels at stations 02OA040 (dashed line) and 02PA005 (solid line), for the period 1964 to 1978. Note the agreement between peaks and troughs of the two time series. Linear regression analysis yields a sample correlation coefficient of 0.9. The source of hydrometric data is the Water Survey of Canada.

Appendix B. Relationship Between Water Levels and Streamflow

The relationship between water levels and streamflow is determined to permit correlation of the present analysis with previously published streamflow versus seismicity analyses for other seismic zones. The data set analyzed were obtained from the Water Survey of Canada and consist of 70 years of daily water level observations at station 02OA040, and 34 years of daily streamflow observations at station 02OA016. Both hydrometric stations are located on the St. Lawrence river, as shown in Figure 15.

A scatter plot of the daily streamflow volume versus water levels, for the 34 years of common observations (1955-1988), is shown in Figure 31. The linearities observed for values of streamflow greater that 10000 m^3/sec are due to change in the daily rate of flow variation. For streamflow volumes less than 10^5 m^3/sec the daily variations are in the order of 10 m^3/sec, whereas for streamflow volumes greater than 10^5 m^3/sec the daily variations are in the order of 10^2 m^3/sec, resulting in the "gaps" observed for large streamflow volumes. Note in Figure 31 that most points, of the total of 12418, show an approximately linear trend, except for some scattered points in the lower right section of the plot. As indicated by the Quebec Historical Streamflow Summary (Environment of Canada, 1989), these scattered points (indicated by the symbol B opposite of the observation) correspond to ice conditions affecting the flow-level relationship. Ice conditions (B) are indicated for all streamflow measurements after 1977. The scatter plot of streamflow versus water level from 1977 to 1988, with the data points corresponding to ice conditions removed, and with a straight line fit, is shown in Figure 32.

Regression analysis is applied to the 34 years of daily water level and streamflow data sets (1977 - 1988), with the points corresponding to ice conditions removed; the model tested is $[flow] = b_0 + b_1[level] + b_2[level]^2 + b_3[level]^3 + \ldots$. The analysis yielded that a linear relationship is a very good approximation, with sample correlation coefficient $r = 0.98$ for the model $[flow] = b_0 + b_1[level]$. Regression analysis of the entire data set (1955 - 1988), including the "ice conditions" points, also indicates that a linear relationship between the two data sets is a good approximation, with correlation coefficient of 0.97. Thus, the two hydrometric data sets, water levels and streamflow, are linearly related, and therefore they would exhibit the same temporal behavior.

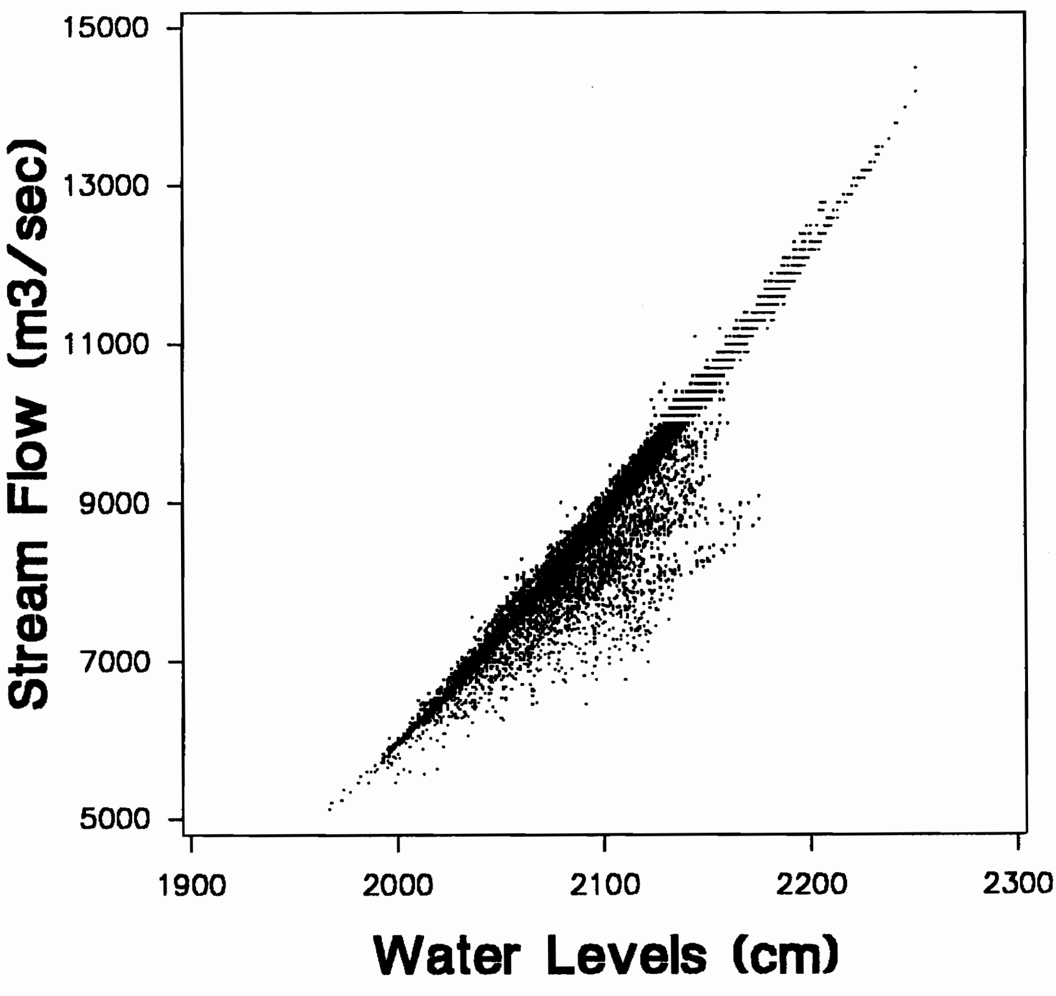

Figure 31. Streamflow vs Water Levels at Stations 02OA016 and 02OA040: Plot of the daily streamflow versus water level data sets for the period 1955 to 1988. Note the scattered points at the lower right section of the plot due to "ice conditions".

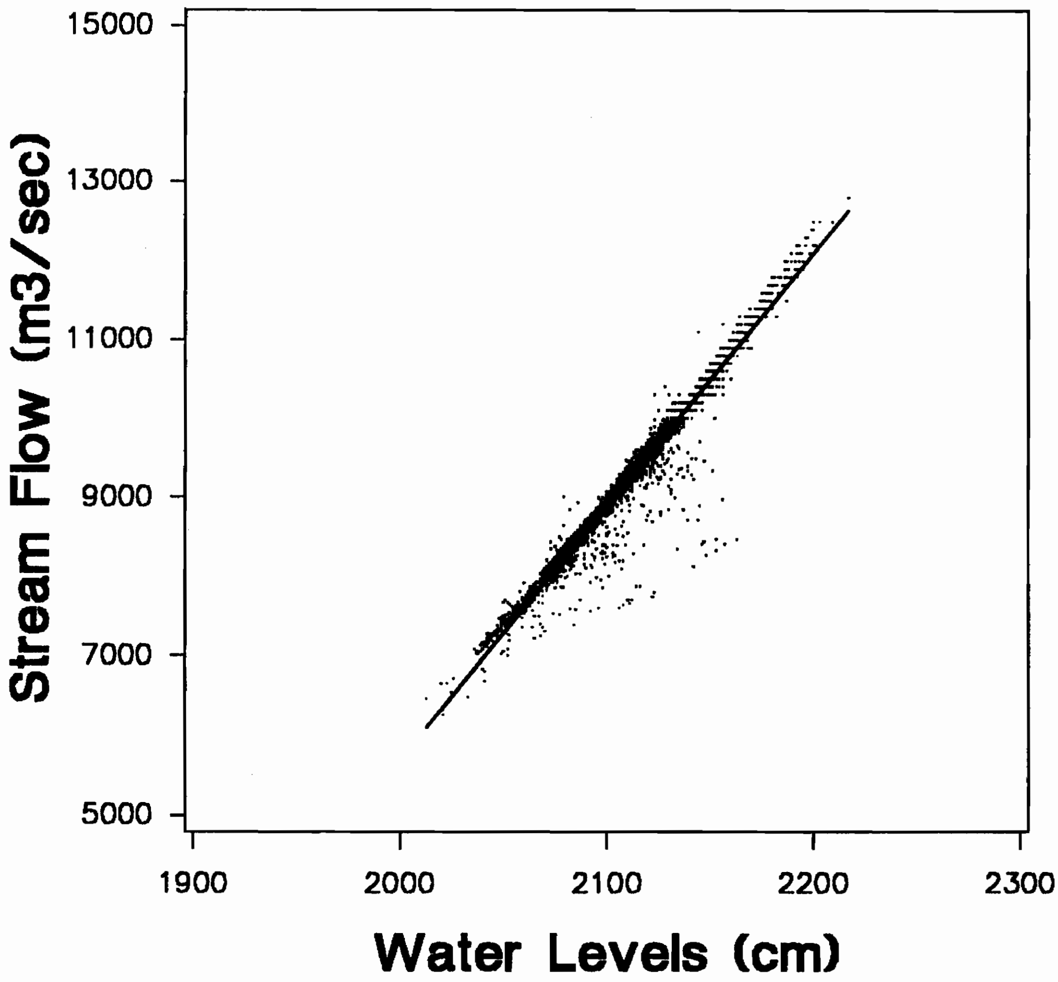

Figure 32. Straight Line Fit to Streamflow vs Water Level Data Sets: Plot of the daily streamflow versus water level data sets for the period 1977 to 1988, with the points corresponding to ice conditions removed, and a least squares straight line fit with a sample correlation coefficient of 0.98.

Vita

George Padelis Tsoflias was born in Athens, Greece on April 26, 1964. He graduated from Lycée Léonin High School in Athens on June 1982 and in September of the same year he was admitted to the National Merchant Marine Academy of Greece. In June 1984 he graduated with a Third Officer's, Captain's Degree. In January 1985 he began his undergraduate career at Mary Washington College, in Virginia, and in September 1986 he transferred to Virginia Tech, from where he received a Bachelor of Science Degree in Geophysics, in June 1989. In August 1989, he begun graduate studies at Virginia Tech and obtained his Masters of Science Degree in Geophysics in August 1991. George Tsoflias became a citizen of the United States in June 1991, and will begin his career as an Exploration Geophysicist for Mobil Oil U.S. in New Orleans, Louisiana, in September 1991.